Derivation of Extra-embryonic and Intra-embryonic Macrophage Lineages from Human Pluripotent Stem Cells

Andrea L. Bredemeyer[1], Junedh M. Amrute[1], Andrew L. Koenig[1], Rachel A. Idol[5], Li He[1], Stephanie A. Luff[6,7], Carissa Dege[2], Jamison M. Leid[1], Joel D. Schilling[1], J. Travis Hinson[3,4], Mary C. Dinauer[5], Christopher M. Sturgeon[2,6,7,#], Kory J. Lavine[1,8,9,#]

[1]Center for Cardiovascular Research, Departmental of Medicine, Cardiovascular Division, Washington University School of Medicine, St. Louis, MO, USA
[2]Department of Medicine, Division of Hematology, Washington University School of Medicine, St. Louis, MO
[3]Departments of Cardiology, Genetics and Genome Sciences, UConn Health, Farmington, CT.
[4]The Jackson Laboratory for Genomic Medicine, Farmington, CT
[5]Department of Pediatrics, Washington University School of Medicine, St. Louis, MO, USA
[6]Department of Cell, Developmental and Regenerative Biology, Icahn School of Medicine at Mount Sinai, New York, NY
[7]Black Family Stem Cell Institute, Icahn School of Medicine at Mount Sinai School of Medicine, New York, NY
[8]Department of Pathology and Immunology, Washington University School of Medicine, St. Louis, MO, USA
[9]Department of Developmental Biology, Washington University School of Medicine, St. Louis, MO, USA

Key words: Macrophages ▪ hematopoiesis ▪ tissue resident macrophages ▪ human pluripotent stem cells

[#]Address for correspondence

Christopher M. Sturgeon, PhD
Icahn School of Medicine at Mount Sinai
Black Family Stem Cell Institute
Mount Sinai School of Medicine
One Gustave L. Levy Place, Box 1496
New York, NY 10029
Phone: 212-659-8278
Fax: 212-659-9653
Email: christopher.sturgeon@mssm.edu

Kory J. Lavine MD, PhD
Center for Cardiovascular Research
Departmental of Medicine
Washington University School of Medicine
660 South Euclid Campus Box 8086
St. Louis, MO, 63110
Phone: 314 362-1171
Fax: 314 362-0186
Email: klavine@wustl.edu

Summary Statement

Generation of intra-embryonic-like and extra-embryonic-like macrophages from human pluripotent stem cells reveals intrinsic differences in macrophages generated through distinct hematopoietic pathways.

Abstract

Tissue resident macrophages are increasingly recognized as important determinants of organ homeostasis, tissue repair, remodeling, and regeneration. While the ontogeny and function of tissue resident macrophages has been identified as distinct from postnatal hematopoiesis, the inability to specify, *in vitro*, similar populations that recapitulate these developmental waves has limited our ability to study their function and potential for regenerative applications. We took advantage of the concept that tissue resident macrophages and monocyte-derived macrophages originate from distinct extraembryonic and definitive hematopoietic lineages to devise a system to generate pure cultures of macrophages that resemble tissue resident or monocyte-derived subsets. We demonstrate that hPSC-derived extra-embryonic-like and intra-embryonic-like hematopoietic progenitors differentiate into morphologically, transcriptionally, and functionally distinct macrophage populations. Single cell RNA sequencing of developing and mature cultures uncovered distinct developmental trajectories and gene expression programs of macrophages derived from extra-embryonic-like and intra-embryonic-like hematopoietic progenitors. These findings establish a resource to generate human tissue resident-like macrophages to study their specification and function under defined conditions and to explore their potential use in tissue engineering and regenerative medicine applications.

Introduction

Macrophages are well appreciated for their roles in pathogen responses, including phagocytosis of pathogens and removal of cellular debris, release of inflammatory cytokines, and presenting antigen to cells of the adaptive immune system (Murray and Wynn 2011). Over the last ten years, however, the impact of macrophages residing within tissues on organ homeostasis and repair has become increasingly understood. Studies of resident macrophages across various tissues have revealed common functions, such as promoting angiogenesis and proper tissue patterning during development (Wynn, Chawla, and Pollard 2013). Each tissue environment also instructs macrophages to take on specific functional properties, leading to specialization of microglia in the brain, Kupffer cells in the liver, Langerhans cells in the skin, and osteoclasts in the bone (Epelman, Lavine, and Randolph 2014; Davies et al. 2013; Lavin et al. 2014).

Tissue-resident macrophages are initially derived from the hematopoietic progenitors arising in the extra-embryonic yolk sac (Hoeffel and Ginhoux 2015; Hoeffel et al. 2015; Ginhoux et al. 2010; Yona et al. 2013). During early embryogenesis these extra-embryonic cells migrate to developing tissues where they establish their tissue-specific identity. Over the course of fetal development and postnatal life, these tissue resident macrophages have the capacity to self-renew and are maintained in the absence of replenishment from monocytes in many tissues, including liver, lung, brain and heart (Hashimoto et al. 2013; Epelman et al. 2014; Ajami et al. 2007). Similarly, upon physiological stressors such as injury or ageing, monocyte-derived macrophages can migrate to these tissues and function as tissue-resident macrophages (Epelman et al. 2014; Daemen et al. 2021). However, these ontogenically-distinct macrophages generally lack the reparative functions of their extra-embryonic-derived counterparts, instead causing inflammation that can contribute to disease phenotypes (Honold and Nahrendorf 2018; Puranik et al. 2018).

Extra-embryonic hematopoiesis in the yolk sac occurs in at least two waves, the first consisting of primitive, c-Myb-independent progenitors that give rise to a very limited set of hematopoietic cells (primitive erythroblasts, megakaryocytes and macrophages) and the second consisting of c-Myb-dependent erythromyeloid progenitors (EMPs) that give rise to erythroid, myeloid, and NK cell lineages (Dege et al. 2020; Frame, McGrath, and Palis 2013; Kasaai et al. 2017; McGrath et al. 2015; Palis, McGrath, and Kingsley 1995; Palis et al. 1999; Palis and Yoder 2001; Lux et al. 2008). EMPs provide the first progenitors that colonize the fetal liver, giving rise to diverse myeloid cells. In contrast, the intra-embryonic hemogenic endothelium within the aorta-gonad-mesonephros (AGM) region gives rise to definitive

multipotent progenitors (MPPs) and hematopoietic stem cells (HSCs). These long-lived HSCs migrate to the fetal liver, and finally the bone marrow, to produce a full assortment of myeloid and lymphoid cells.

In order to assess the intrinsic differences between hematopoietic lineages arising from extra- and intra-embryonic hematopoiesis, we developed an *in vitro* human pluripotent stem cell (hPSC) differentiation model of hematopoiesis that recapitulates these anatomically distinct hematopoietic programs. By manipulating WNT signaling at an early stage of differentiation, we can generate either exclusively extra-embryonic-like (WNT-independent, WNTi) CD34+ hematopoietic progenitors, or exclusively intra-embryonic-like (WNT-dependent, WNTd) CD34+ hematopoietic progenitors (Sturgeon et al. 2014). WNTi progenitors lack the expression of *HOXA* genes and have restricted erythro-myeloid potential, mirroring extra-embryonic hematopoiesis, while WNTd progenitors express *HOXA*, and display multi-lineage erythro-myelo-lymphoid potential, recapitulating intra-embryonic-like MPP development (Ng et al. 2016).

Herein, we present a platform to generate two ontogenically distinct myeloid populations from hPSCs. Through our ability to directly compare each population from a single isogenic source, we demonstrate that macrophages differentiated from extra-embryonic-like (WNTi) and intra-embryonic-like (WNTd) hematopoietic progenitors harbor distinct transcriptional signatures, morphologies, developmental pathways, and functions, which recapitulate the general properties observed in yolk sac-derived and intra-embryonic macrophages, respectively. These findings establish a robust *in vitro* system to generate functionally distinct myeloid populations for investigation of human macrophage specification, differentiation, function, and regenerative potential.

Results

Generation of macrophages derived from extraembryonic- and intraembryonic-like hematopoietic progenitors. Using previously described conditions to exclusively specify extra-embryonic-like and intra-embryonic-like hematopoietic progenitors from hPSCs, we sought to determine whether we could generate functional macrophages in these lineages (**Fig. 1A**). Consistent with previous findings, differentiation under WNT-independent (WNTi) conditions (IWP2 treatment) gave rise to CD34+ progenitors that rapidly transitioned to CD43+ hematopoietic progenitors by day 8 of differentiation. Within these cultures, CD34-CD43+ cells displayed predominantly erythroid potential, while CD34+CD43+ cells instead harbored robust myeloid potential, identifying them as a candidate population of extra-embryonic-like macrophage progenitors (**Fig. S1A-B**). In contrast, treatment with GSK3 inhibitor CHIR99021, which activates WNT (and consequently Notch) signaling, and TGFβ inhibitor SB431542 (called WNT-dependent, or WNTd, conditions here for simplicity), yields CD34+CD43-CD73-CD184- hemogenic endothelial cells on day 8 of differentiation, which possess intra-embryonic-like erythroid, myeloid and lymphoid multipotent potential (Ditadi et al. 2015; Ng et al. 2016).

WNTi CD34+CD43+, WNTd CD34+CD43-CD73-CD184-, and human cord blood (CB) CD34+ populations were isolated by FACS, then cultured under serum-free conditions supplemented with M-CSF and additional cytokines to drive macrophage differentiation (**Fig. S1A**). CB CD34+ hematopoietic progenitors were used as a control for definitive hematopoiesis. After 14 days, the cultures were analyzed by flow cytometry for expression of leukocyte marker CD45 and common macrophage markers. Differentiation in all cultures was highly efficient, as over 90% of the cells expressed CD45 and the macrophage markers CD14 and MertK (**Fig. 1B**). The WNTd culture yielded an average of $2x10^6$ macrophages per $1x10^5$ purified progenitors, while the WNTi culture averaged $1x10^6$ macrophages per $1x10^5$ sorted progenitors. WNTi and WNTd cultures were each generated from $5x10^6$ hPSCs. While the cells within the WNTd- and CB-derived cultures had similar scatter properties, WNTi-derived cells displayed higher median forward scatter (FSC) and side scatter (SSC) (**Fig. 1C, Fig. S1C**). We also examined CCR2 expression in each population, as its expression on tissue-resident macrophages correlates with an intra-embryonic, but not extra-embryonic, origin (Bajpai et al. 2018; Epelman

et al. 2014). Consistent with an extra-embryonic-like origin, WNTi CD45+CD14+ cells were completely devoid of CCR2 expression, while the WNTd- and CB-derived cells both exhibited CCR2+ and CCR2- subsets (**Fig. 1D)**. Electron microscopy revealed that the cells from each culture contained morphological elements typical of macrophages, including phagosomes, lysosomes, and pseudopodia (**Fig. 1E)**. Finally, we assessed the phagocytosis efficiency of each population by culturing the cells with pHrodo Red *E. coli* BioParticles, which will only fluoresce in low pH phagosomes. Both the WNTi and WNTd macrophages had similar percentages (comparable to CB-derived macrophages) and levels of pHrodo Red positivity, demonstrating comparable phagocytic capacity for *E. coli* particles (**Fig. 1F, Fig. S1D)**. Collectively, these phenotypic analyses indicate that each CD45+ population is comprised of macrophages, with hPSC-derived WNTd macrophages displaying strong similarity to those derived from CB HSPCs, while WNTi macrophages are phenotypically unique.

Distinct Transcriptomic Signatures in WNTi and WNTd macrophages. Monocyte-derived macrophages and yolk-sac-derived tissue resident macrophages have distinct gene expression profiles. However, the extent to which these gene expression differences are cell intrinsic or driven by their environment remains incompletely understood. As our *in vitro* platform yields macrophages from extra- and intra-embryonic-like progenitors, we asked whether each population harbors gene expression differences, at single-cell resolution. 11,113 cells from macrophage day 14 cultures were captured for single cell RNA sequencing (scRNAseq). Both WNTd and WNTi samples had comparable numbers of genes and unique molecular identifiers (UMIs) per cell (**Fig. S2A**). Unsupervised clustering of the WNTi and WNTd macrophages together by Uniform Manifold Approximation and Projection (UMAP) identified 12 cell clusters, with the WNTd and WNTi cells predominantly segregating into distinct groups of clusters (**Fig. 2A-B, Fig. S2B**). Differentially enriched genes (DEGs) within each cluster allowed for the identification of cell fate (**Fig. 2C, Table S1**). While most cells were in G0/G1 across both datasets, we also identified a separate cluster with enriched expression of S/G2/M-associated genes (*TOP2A, KIAA0101, MKI67, CDK1*; **Fig. 2B-C, Fig. S2B-C**).

Macrophages were identified based on expression of *SPP1, C1QA, C1QB* and *C1QC* and made up most clusters in both the WNTi and WNTd populations (**Fig. 2C**). The WNTd and WNTi macrophages also expressed comparable levels of *MAF*, *MAFB*, *CD68*, *CD163*, and *MRC1* (**Fig. S2D-E**). In contrast, a cluster of cells expressing characteristic monocyte genes (*FCN1, CD52, LYZ,* and *PLAC8*), as well as CCR2, was found exclusively in the WNTd culture (**Fig. 2C** and **Fig. S2F**). We also identified a small cluster expressing mast cell genes (*KIT, TPSB2, CPA3, HPGD*) in the WNTi culture. At a broad level, the WNTd and WNTi macrophages each expressed a distinct gene signature that spanned all their respective clusters (**Fig. 2D-E, Fig. S3)**. Interestingly, the WNTi macrophage signature includes *LYVE1, F13A1, GAS6, FOLR2, IGFBP4* and *CD36*, genes that are enriched in a variety of tissue-resident macrophages (Summers, Bush, and Hume 2020). The WNTd macrophages, in contrast, expressed a broader repertoire of macrophage-associated genes that regulate function in disease states, such as *TREM2, BTG1, ALDH2, ALOX5AP* and *BNIP3* (**Fig. 2D-E, Fig. S3)** (Corjay et al. 1998; Zhong et al. 2019; Ee et al. 2016; Back et al. 2007; Byrum et al. 1997; Frank et al. 2015; Zhang and Ney 2009). In particular, TREM2 is expressed on macrophages in a variety of disease contexts, including cancer and atherosclerosis, so it is intriguing to find it present across the WNTd macrophage population (Cochain et al. 2018; Deczkowska, Weiner, and Amit 2020; Katzenelenbogen et al. 2020). Differences in protein expression of LYVE1 and TREM2 were confirmed by immunofluorescence (**Fig. S4A-B**). KEGG pathway analysis revealed differences in lysosomal, inflammatory, metabolic, and protein synthetic processes between WNTi and WNTd macrophage populations (**Fig. 2F**).

We identified each macrophage cluster by the top differentially enriched gene (**Fig. 2B and G, Table S1**). The WNTd culture contained five clusters of cells with distinct gene expression signatures, revealing the variety of fates these cells can take on. The *TREM2*^{hi} macrophage cluster expresses the WNTd signature described above, without an

additional unique set of genes, suggesting that this may be the initial state of the WNTd macrophages. The cells in the metallothionein (MT) state express high levels of metallothionein 1 and 2 (MT1 and MT2) genes, which can promote inflammatory responses to pathogens (Subramanian Vignesh and Deepe 2017). The amphiregulin (*AREG*) cluster expresses a set of genes (*AREG, THBS1, RGS2, ABHD2*) that have been shown to promote wound healing and angiogenesis in different tissue injury contexts (Hamidzadeh et al. 2020; Minutti et al. 2019; Zaiss et al. 2015; Kyriakides and Maclauchlan 2009; Boelte et al. 2011; Jin et al. 2009). The *WSB1* (WD Repeat and SOCS Box Containing 1) cluster is also characterized by expression of genes (*WSB1, PNISR, VMP1, N4BP2L2*) that can modulate immune responses and cellular function, including response to hypoxia and autophagy (Grasso et al. 2011; Haque et al. 2016). The MMP12 cluster is characterized almost entirely by expression of *MMP12*, a protease involved in macrophage migration, which is not expressed in the other clusters (Collison 2018).

WNTi macrophages were predominantly contained in a single major cluster (*LYVE1*^{hi}) expressing the WNTi signature discussed above, with minor clusters (<5% of cells) also expressing higher levels of type 1 interferon stimulated genes (interferon state) or chemokines CCL3, CCL4 and CXCL8 (CCL3 state) (**Fig. 2B and G**). The WNTi macrophages also had a small cluster expressing increased levels of a subset of mitochondrially encoded genes (**Fig. S4C**). Analysis of variation in gene expression within the WNTd and WNTi macrophages revealed greater heterogeneity in gene expression in the WNTd macrophages, suggesting that WNTd macrophages can take on a larger number of gene expression states than the WNTi macrophages, reminiscent of the wide variety of fates recruited macrophages take on in response to tissue injury and disease (**Fig. S4D**) (Bajpai and Lavine 2019; Bajpai et al. 2018). Taken together, these observations demonstrate that the WNTi and WNTd macrophages we obtain exhibit different intrinsic gene expression programs, and that these differences parallel those observed between macrophages derived from extra-embryonic and intra-embryonic hematopoietic programs *in vivo*.

Differing developmental pathways underlie the specification of WNTi and WNTd myeloid progenitors. *In vivo*, extra- and intra-embryonic macrophages follow distinct developmental trajectories, with only intra-embryonic myelopoiesis developing through a monocyte stage. As our scRNAseq analyses showed that WNTd, but not WNTi, macrophage cultures contained a monocytic-like precursor, we next asked whether the hPSC myeloid populations we obtain exhibit a similar developmental progression. First, we analyzed the expression of the common monocyte and macrophage markers CD64 (FCGR1A) and CD14 on the developing macrophage cultures, from days 5 through 7, as these timepoints captured developmental intermediates not present in our terminally differentiated cultures. Both cultures exhibited an asynchronous maturational profile, consisting of CD64-CD14-, CD64+CD14-, and CD64+CD14+ populations (**Fig. 3A**). WNTd progenitors exhibited a progressive development through successive stages, first acquiring CD64 expression and then CD14, as suggested by their relative distribution over time. The distribution of these populations remained relatively static in the WNTi cultures at these timepoints, with a slight increase in CD64-CD14- cells and a decrease in CD64+CD14- cells, making it difficult to assess the relationships between these populations using these markers.

To further characterize their development, we assessed each population for the expression of IL3Rα (CD123), which is expressed on common myeloid progenitors (CMPs), and for CD45RA, which is expressed together with IL3Rα on downstream granulocyte/macrophage progenitors (GMPs; (Manz et al. 2002)). Consistent with our assessment of WNTd culture maturation, the CD64-CD14- cells predominantly expressed only IL3-Rα, as observed in CMPs, while the majority of the CD64+CD14- cells expressed both IL3-Rα and CD45RA, similar to GMPs. The fully committed CD64+CD14+ cells all expressed both IL3-Rα and CD45RA (**Fig. 3B**). The pattern of IL3-Rα and CD45RA expression differed, however, in the WNTi culture. The CD64-CD14- population was predominantly negative for IL3-Rα and CD45RA,

while approximately half of the CD64+CD14- cells expressed IL3-Rα. Intriguingly, CD45RA was not detected in either CD14- population, although the CD64+CD14+ macrophages expressed high levels of both IL3-Rα and CD45RA (**Fig. 3B**). Exclusion of erythroid (CD235A+) and megakaryocyte (CLEC1B+) lineage cells increased the percentage of IL3-Rα+ cells, but failed to increase the percentage of CD45RA+ progenitors (**Fig. S5A)**. As this expression pattern suggested an absence of a canonical GMP-like stage, we also assessed an earlier timepoint of myeloid development. At day 3, fewer than 5% of the cells are CD64+CD14+ macrophages, indicating that the macrophage progenitors are still present in the culture. Analysis of the CD14- cells showed that about 40% expressed IL-3Rα and all were negative for CD45RA (**Fig. S5B**). These results suggest that the WNTi macrophage progenitors either do not pass through a canonical GMP progenitor state, or that they pass through this state too rapidly to be detected by flow cytometry.

To further assess the differences between WNTd and WNTi progenitors, we performed scRNAseq on each culture after 6 days in macrophage-inducing media. Based on our flow cytometry, we predicted that both cultures would contain a mixture of cells at different stages of differentiation at this timepoint. We obtained data on 4,217 and 6,994 cells for these WNTi and WNTd progenitor cultures, respectively. Both samples had comparable numbers of genes and UMIs identified per cell (**Fig. S6A**). Using unsupervised clustering of the WNTi and WNTd samples together, we identified 12 distinct clusters (**Fig. 3C-D**). We assigned cluster identities using markers characteristic of hematopoietic cell types and verified them by reference mapping our datasets to integrated human yolk sac and fetal liver scRNAseq data (**Fig. 3E, Fig. S6B-D, Fig. S7A**) (Bagger, Kinalis, and Rapin 2019; Popescu et al. 2019). We also examined gene expression of *IL-3RA*, *FCGR1A*, and *CD14* to correlate the scRNAseq data with our flow cytometry populations, and proliferation markers *MKI67* and *TOP2A* to ensure cell cycle regression was successful (**Fig. S7B-C)**. At this early stage of differentiation, multiple cell types were present in both cultures, giving insight into the overall potential of the WNTd and WNTi progenitors. Both cultures contained clusters expressing canonical monocyte (*PLAC8, LSP1, ASGR2, CORO1A)* and macrophage (*SPP1, VSIG4, C1QA, C1QB, C1QC*) genes; these comprised the majority of the WNTd culture and a smaller fraction of the WNTi culture (**Fig. 3C-F, Fig. S6B-C, Table S2**). None of these clusters expressed high levels of *FUT4*, the gene encoding the neutrophil marker CD15 (**Fig. S7B**). The macrophages present in the WNTi culture predominantly clustered into the Mac-1 cluster. These express higher levels of several genes (including *LYVE1, SIGLEC1, LILRB5, F13A1, CD163* and *DAB2*) than the predominantly WNTd Mac-2 cluster, demonstrating that their gene expression signatures diverge early in macrophage maturation (**Fig. 3C-F, Fig. S6C**). Both cultures also had cells expressing characteristic eosinophil genes (*CLC, IL5RA, EPX, PRG2, PRG3*). Megakaryocyte (*GP9, ITGA2B, PDLIM1* and *PF4*) and mast cell (*KIT, TPSB2,* and *GATA2*) clusters were present primarily in the WNTi culture (**Fig. 3C-F, Fig. S6B, D**). Similarly, the WNTi culture contained a large number of red blood cell (RBC) progenitors, expressing glycophorin A (*GYPA*), *GATA1*, and *KLF*, which were largely absent from the WNTd culture, consistent with an EPO-independent development of the primitive erythroid lineage (Malik et al. 2013). Only the WNTd culture contained a cluster expressing canonical dendritic cell genes (*CD1C, FGL2, ITGB7, CLEC4A*, and *HLA-DRA*, as well as a CD34+ progenitor cluster that expresses characteristic intra-embryonic MPP genes (*MECOM, SPINK2, MLLT3, HLF*) (**Fig S6D** and **S7D**) (Kataoka et al. 2011; Zeng et al. 2019; Pina et al. 2008; Yokomizo et al. 2019). To further verify that the WNTd culture represents intra-embryonic-like hematopoiesis, we reference mapped human fetal liver HSC/MPPs and yolk sac MPPs onto our WNTd progenitor dataset (Popescu et al. 2019). The fetal liver HSCs mapped strongly to the WNTd CD34+ progenitors, while the yolk sac MPPs did not (**Fig. S7E**). In particular, the human fetal liver HSC/MPPs and the WNTd CD34+ progenitors express *HOXA9*, which is absent in the human yolk sac progenitors and the WNTi cells (**Fig. S7F**) (Popescu et al. 2019). *HOXA9* has previously been shown to be a critical factor for generation of HSCs from endothelium (Zhou et al. 2016; Ng et al. 2016).

Interestingly, WNTi and WNTd cultures both contained cells expressing canonical GMP genes (*ELANE, MPO, AZU1, PRTN3*), despite the WNTi culture not having a classical CD45RA+ GMP population by flow cytometry (**Fig. 3F, Fig. S6C**). Thus, we further investigated the macrophage progenitor populations in each culture via pseudotime analysis

using Palantir (Setty et al. 2019). We independently clustered the WNTd and WNTi progenitor datasets, assigned cluster identifications using the gene sets shown in **Fig. S6**, and superimposed pseudotime and entropy values (**Fig. 4, Fig. S8A-B**). We additionally plotted the probability of a cell differentiating into a macrophage or dendritic cell to identify the developmental trajectory of this lineage. Within the WNTd differentiation, CD34+ progenitors displayed the lowest pseudotime and greatest entropy values, consistent with these cells being the earliest population (**Fig. 4A-B**). Calculation of macrophage and dendritic cell potential showed the expected developmental trajectory from GMP to monocyte to macrophage/dendritic cell (**Fig. 4C**). Interestingly, we found two separate WNTd monocyte populations; monocyte-1 falls between the GMP and macrophage clusters, while monocyte-2 falls between the CD34+ progenitor and dendritic cell-like clusters (**Fig. 4A, Fig. S8A**). Monocyte-2 cells express several genes found in human dendritic cells, including *ENHO, CD1D, ITGB7, FGL2* and *CLEC10A*, indicating that these monocytes are likely dendritic cell progenitors. This observation is consistent with the finding in mice that monocyte-derived dendritic cells come from a monocyte-dendritic cell progenitor (MDP) that arises directly from the common myeloid progenitor (CMP), rather than from the GMP(Yanez et al. 2017). The monocyte-2 gene signature is absent from the WNTi culture, consistent with the lack of a WNTi dendritic cell-like population (**Fig. S8B**).

The WNTi clusters with the lowest pseudotime and highest entropy values included RBC progenitors and a population of potential myeloid progenitors that clustered between megakaryocytes and monocytes (progenitor 1, **Fig. 4D-E**). Calculation of macrophage potential suggested that progenitor 1 has the capacity to give rise to macrophages (**Fig. 4F**). This analysis also showed possible macrophage potential arising out of the eosinophil cluster, which contained cells expressing GMP genes (*ELANE, MPO, AZU1, PRTN3*) (progenitor 2, **Fig. 4D, F-G**). To determine whether these two progenitors can give rise to macrophages, we established a flow cytometry protocol to isolate these cell populations. Based on the scRNAseq data, we found that *CXCR4* was expressed in both progenitor 1 and 2 (**Fig. 4H)**. As *CXCR4* is also expressed in the WNTd GMP cluster, it may be a useful marker of macrophage progenitors (**Fig. S8C**). The progenitor 1 cluster also expressed megakaryocyte marker *CLEC1B*. We isolated CD14-CXCR4+CLEC1B- and CD14-CXCR4+CLEC1B+ cells from macrophage day 4 WNTi differentiations and cultured them in macrophage media for 7 days. The CXCR4+CLEC1B- and CXCR4+CLEC1B+ cells both efficiently gave rise to CD14+ cells with similar morphology, confirming their macrophage potential (**Fig. 4I and Fig. S8D**). Addition of stem cell factor (SCF) to macrophage media supported mast cell differentiation from both progenitor 1 and 2 (**Fig. S8E**). Culture in megakaryocyte-inducing conditions gave rise to CD41+CD42b+ megakaryocytes from both progenitors, with a higher percentage of CD41+CD42b+ cells in the progenitor 1 culture (**Fig. S8F)**. When cultured under conditions supporting granulocyte differentiation, progenitor 2 gave rise to CD32+CD15+CD16+ neutrophils, consistent with the expression of GMP genes in this cluster, while no CD32+ granulocytes arose from progenitor 1 (**Fig. S8G-H**).

To confirm that the WNTi cells expressing GMP genes were not due to contamination from the WNTd pathway, we isolated KDR+CD235A+ cells on day 3 of a WNTi differentiation, which have previously been shown to have exclusively extra-embryonic-like hematopoietic potential (**Fig. S9A**) (Sturgeon et al. 2014). We also isolated KDR+CD235A- cells from a WNTd culture, which are exclusively intra-embryonic-like, at the same timepoint. These cells were differentiated as before, then CD34+CD43+ WNTi cells and CD34+CD43- WNTd cells were isolated on Day 8 and cultured in macrophage media (**Fig. S9B**). After six days of macrophage differentiation, we analyzed MPO protein expression, as a marker of the GMP gene program, and found MPO+CD14- cells in the WNTi and the WNTd cultures, (**Fig. S9C**). Therefore, while WNTi progenitors may not pass through a canonical GMP, based on surface expression of CD45RA, the cells arising from progenitor 2 nevertheless develop through a transitional intermediate that expresses a GMP-like gene signature. Progenitor 1, in contrast, does not contain a GMP-like population, but instead has a gene expression profile comparable to the EMP and pre-macrophages (pMac) observed in mice (**Fig. 4J-K, Table S3.**)(Mass et al. 2016).

WNTi and WNTd macrophages are functionally distinct. We next sought to determine whether WNTi and WNTd macrophages exhibit functional differences. Tissue resident macrophages express lower levels of inflammatory genes in response to stimuli, as compared to monocyte-derived macrophages(Watanabe et al. 2019; Epelman et al. 2014; Lavine et al. 2014). To determine whether WNTi and WNTd macrophages had intrinsically different inflammatory responses, we assayed levels of *IL-1β*, *TNFα* and *IL-6* gene expression following treatment with lipopolysaccharide (LPS). Upon stimulation with either 2.5 ng/mL or 25 ng/mL LPS, WNTi macrophages expressed significantly lower levels of *IL-1β* and *TNFα* than WNTd macrophages, while expression of *IL-6* was comparable between the two (**Fig. 5A**). Thus, in the context of LPS treatment, WNTi macrophages appear to be less inflammatory than WNTd macrophages.

As shown in Fig. 1, phagocytosis of *E. coli* particles was not different between WNTd and WNTi macrophages, but higher expression of *CD36* on WNTi macrophages indicated possible increased phagocytic capacity for apoptotic cells. To test this hypothesis, we incubated WNTi and WNTd macrophages with pHrodo Red-labeled apoptotic mouse thymocytes. After 2 or 5 hours of co-incubation, we assayed the number of thymocytes phagocytosed by each macrophage (**Fig. 5B**). At both time points, a higher percentage of WNTi macrophages had phagocytosed thymocytes, as compared to the WNTd macrophages. Additionally, the mean number of thymocytes phagocytosed by each WNTi macrophage was higher, yielding a higher overall phagocytic index for apoptotic cells (**Fig. 5B-C**).

Production of reactive oxygen species (ROS) by macrophages is a critical component of their role in clearance of pathogens; however, it can also modulate immune responses and promote polarization of macrophages toward a reparative phenotype (Yang et al. 2019). Thus, we wanted to determine whether there are intrinsic differences in ROS production between WNTi and WNTd macrophages. We stimulated WNTi and WNTd macrophages with either serum opsonized zymosan (SOZ) particles or phorbol 12-myristate 13-acetate (PMA) and used a luminol-based assay to detect production of ROS. WNTi macrophages produced significantly more ROS than WNTd macrophages in response to SOZ, but there was no difference in response to PMA, suggesting a specificity for increased ROS production in WNTi macrophages in response to a particulate antigen (**Fig. 5D**). A nitroblue tetrazolium (NBT) assay to detect ROS producing cells microscopically showed no difference in the number of NBT+ cells (data not shown). We also did not find differences in the expression of NADPH oxidase NOX2 (*CYBB*) or potential SOZ receptors Toll-like receptor 2 (*TLR2*), Mac-1 (*ITGB2*) or dectin (*CLEC7A*) between WNTi and WNTd macrophages (**Fig. S10A**). Intriguingly, it has previously been shown that mouse resident peritoneal macrophages have a sustained respiratory burst in response to zymosan that is dependent on generation of ROS by the mitochondrial respiratory chain (Davies et al. 2017). The peritoneal macrophages also had increased mitochondrial respiratory capacity, when compared to bone marrow derived macrophages (BMDMs), that allowed for this sustained respiratory burst. Thus, we assayed mitochondrial function in the WNTi and WNTd macrophages by measuring oxygen consumption rate (OCR) during a mitochondrial stress test. WNTi macrophages had a higher basal OCR and showed higher spare respiratory capacity (SRC) upon electron transport chain uncoupling than WNTd macrophages (**Fig. 5E-F**). This phenotype was amplified upon treatment with LPS. A subset of mitochondrially encoded components of the electron transport chain (*MT-ND4, MT-ND5, MT-CO2, MT-CYB*) are expressed at higher levels in WNTi macrophages, as compared to WNTd macrophages, which may contribute to this increased respiratory capacity (**Fig. S10B**). Collectively, these data indicate that WNTi and WNTd macrophages have inherent differences in metabolic and inflammatory capacity that are consistent with known functional distinctions between tissue resident and monocyte-derived macrophages.

Discussion

Tissue resident macrophages are increasingly recognized as important contributors to embryonic development, tissue maturation, remodeling and repair. To date, few systems exist to investigate tissue resident macrophage specification, function, and applicability to regenerative medicine. This technological gap is most apparent in the study of human tissue resident macrophages, which is largely restricted to *ex vivo* and transcriptomic analyses of explanted human specimens. Recent reports have demonstrated that macrophages derived from iPSCs though yolk-sac-like hematopoiesis can take on microglial characteristics when co-cultured with neurons, but these have not been compared with macrophages generated through intra-embryonic-like hematopoiesis (Takata et al. 2017; Haenseler et al. 2017). By leveraging known differences in the developmental origin of tissue resident and monocyte-derived macrophages, we established an experimentally tractable *in vitro* system to model each of these macrophage populations. We demonstrate that macrophages derived from extra-embryonic-like and intra-embryonic-like hematopoietic progenitors have unique gene expression signatures, developmental trajectories, and functions that are consistent with *in vivo* characteristics of tissue resident and monocyte-derived macrophages, respectively.

Differences between tissue-resident macrophages and monocyte-derived macrophages have been largely ascribed to the impacts of the tissue microenvironment (Lavin et al. 2014). While the tissue environment is certainly a major component driving behavior of tissue-resident macrophages, we show intrinsic differences in transcriptional signatures and cellular function between extra- and intra-embryonic-like macrophage lineages. We revealed that macrophages derived from extra-embryonic-like hematopoiesis (WNTi) express a wide array of genes associated with general tissue-resident macrophage identity (Summers, Bush, and Hume 2020). These genes are expressed in multiple types of tissue-resident macrophages, as well as in human yolk-sac derived macrophages isolated prior to hematopoietic stem cell (HSC) formation, suggesting that the extra-embryonic macrophages that populate tissues during development are predisposed to this gene expression program (Bian et al. 2020; Popescu et al. 2019). Genes that are associated with a specific type of tissue-resident macrophage, such as Kupffer cell-associated *CLEC4A* and *CD5L* and Langerhans cell-associated *CD207*, were largely absent from both WNTi and WNTd macrophages (Summers, Bush, and Hume 2020).

WNTi and WNTd macrophages emerge from distinct progenitors, each with different functional capacity. The WNTd progenitors recapitulate definitive myelopoiesis, with eosinophil and megakaryocyte lineages completely separate from the monocyte and macrophage lineage, consistent with these cell types originating from distinct CMPs (Drissen et al. 2016; Drissen et al. 2019). In contrast, the WNTi GMP-like progenitor (progenitor 2) also expressed eosinophil genes. Additionally, WNTi progenitor 1 expresses megakaryocyte genes, as has been described for yolk-sac-derived EMPs (Mass et al. 2016). This overlap between transcriptional programs in the WNTi progenitors may drive differences in gene expression and cellular function between WNTi and WNTd macrophages. The expression of *MYB* in both WNTi progenitors, the similarity of progenitor 1 to the mouse EMP, and the diversity of myeloid cell types present in the WNTi culture all support the conclusion that the WNTi culture recapitulates the EMP wave of yolk sac hematopoiesis that gives rise to the majority of fetal tissue resident macrophages (Hoeffel et al. 2015).

Our results further demonstrate functional differences between WNTi and WNTd macrophages that may have relevance for the function of extra- and intra-embryonic-derived macrophages *in vivo*. Previous studies have shown that metabolic changes in macrophages can alter their inflammatory properties. The mitochondrial capacity we observe in WNTi macrophages recapitulates the phenotype of resident peritoneal macrophages, which are established during embryogenesis and self-renew during adulthood (Yona et al. 2013). These peritoneal macrophages have higher spare respiratory capacity than BMDMs, despite not having a greater number of mitochondria, and utilize different metabolites (Davies et al. 2017). Resident peritoneal macrophages also have higher oxygen consumption and higher ROS production in response to zymosan, and the increase in ROS was sensitive to inhibition of the mitochondrial electron

transport chain (Davies et al. 2017). This study supports the possibility that metabolic differences underlie the observed increases in ROS production and spare respiratory capacity in WNTi macrophages.

In conclusion, we establish a human platform to generate distinct lineages of macrophages derived from extra-embryonic-like and intra-embryonic-like progenitors that resemble tissue resident and monocyte-derived macrophages, respectively. This system is experimentally tractable, as it produces large numbers of cells from a renewable resource and is amenable to pharmacologic and genetic manipulations. We envision that this platform will provide new opportunities to explore applications of human tissue resident macrophages to regenerative medicine and to dissect the mechanisms that underlie tissue resident macrophage specification, differentiation, and function.

Materials and methods

hPSC Culture and Differentiation

The hESC line, H1, (WA01; WiCell; male) was maintained on irradiated mouse embryonic fibroblasts in hESC media, as described previously (Sturgeon et al. 2014). For differentiation, hPSCs were cultured on Matrigel-coated plasticware (BD Biosciences) for 24 h, followed by embryoid body generation. Briefly, hPSCs were dissociated with trypsin-EDTA (0.05%) treatment for 1 minute, and cells were detached by scraping to form small aggregates (6-10 cells). Embryoid bodies were resuspended in SFD (Sturgeon et al. 2012) supplemented with L-glutamine (2 mM), L-ascorbic acid (1 mM), monothioglycerol (MTG, $4x10^{-4}$ M), holo-transferrin (150 µg/mL) and BMP4 (10 ng/mL). After 24 hours, bFGF (5 ng/mL) was added to the media. At 42 hours of differentiation, Activin A (1 ng/mL) and either CHIR99021 (3 µM) and SB431452 (6 µM) (to specify WNT-dependent hematopoietic progenitors) or IWP2 (3 µM) (to specify WNT-independent hematopoietic progenitors) were added to the culture. At 72 hrs of differentiation, embryoid bodies were washed with IMDM (ThermoFisher) to remove WNT modulating small molecules and placed in StemPro-34 (ThermoFisher) supplemented with L-glutamine (2 mM), ascorbic acid (1 mM), monothioglycerol (MTG, 4x10-4 M), holo-transferrin (150 µg/mL), VEGF (15 ng/mL) and bFGF (5 ng/mL). On day 6 of differentiation, IL-6 (10 ng/mL), IL-11 (5 ng/mL), and SCF (50 ng/mL) were added to the culture. Cultures were maintained in a low oxygen, 5% CO2/5% O2/90% N2 incubator. All human recombinant factors and small molecules were purchased from R&D Systems. On day 8 of differentiation, hematopoietic progenitors were isolated by fluorescence activated cell sorting (FACS) on a BD FACSAria. CD34-PE/Cy7 (clone 8G12, Cat# 348791), CD43-FITC (clone 1G10, Cat# 555475), CD184-APC (clone 12G5, Cat# 555976) and CD73-PE (clone AD2, Cat# 550257) antibodies were all purchased from BD Biosciences. Human cord blood CD34+ progenitors were isolated using CD34-APC (clone 8G12, Cat# 340441) from BD Biosciences.

Derivation of myeloid cells from hPSC Hematopoietic Progenitors

Isolated WNT-dependent progenitors (CD34+CD43-), WNT-independent progenitors (CD34+CD43+), and umbilical cord blood progenitors (CD34+) were added to Matrigel-coated wells of a 24-well plate in StemPro-34 media (supplemented with L-glutamine, ascorbic acid, MTG and holo-transferrin as above) containing TPO (30 ng/mL), BMP4 (10 ng/mL), IL-6 (10 ng/mL), IL-11 (5 ng/mL), FLT3L (10ng/mL), M-CSF (10 ng/mL), bFGF (5 ng/mL) and VEGF (5 ng/mL). These cells were cultured for 14 days to generate mature macrophages. For generation of additional myeloid cell types from WNTi P1 and P2, cells sorted on Mac Day 4 were cultured in media containing 50 ng/mL SCF (mast cells); 50 ng/mL G-CSF, 25 ng/mL IL-3 and 1 ng/mL IL-5 (granulocytes); or 50 ng/mL TPO and 25 ng/mL SCF (megakaryocytes). Granulocyte formation was also assessed by seeding $1x10^4$ P1 and P2 cells in 10mL MethoCult H4034 (Stemcell Technologies) for 9 days.

Flow Cytometry of Myeloid Progenitors and Macrophages

WNTd and WNTi myeloid progenitors were isolated by harvesting all non-adherent cells on days 5-7 of macrophage differentiation. Cells were analyzed by flow cytometry using CD123-APC (clone 6H6, Cat# 306011), CD45RA-APC/Cy7 (clone HI100, Cat# 304127), CD64-FITC (clone 10.1, Cat# 305006), and CD14-PE (clone M5E2, Cat# 301806) antibodies from Biolegend. For characterization of macrophage progenitor potential, cells were harvested on day 4 of macrophage differentiation as above, then isolated by FACS using CXCR4-APC (clone 12G5, Cat# 306509) and CLEC1B-FITC (clone AYP1, Cat# 372007) antibodies from Biolegend. Other myeloid cell types were analyzed using KIT-BV421 (clone 104D2, Biolegend Cat# 313215), CD15-APC (clone HI98/HIM1, BD Cat# 551376), CD16-PerCP-Cy5.5 (clone 3G8, BD Cat# 560717), CD32-PE (clone FUN-2, Biolegend Cat# 303206), CD41a-PE (clone HIP8, BD Cat# 555467), CD42b-APC (clone HIP1, Biolegend Cat# 303912). For analysis of MPO expression, cells were harvested on day 6 of macrophage differentiation, fixed and permeabilized using Fix&Perm Cell Permeabilization Kit from ThermoFisher (Cat# GAS004), then stained with MPO antibody (clone MPO455-8E6, Cat# 12-1299-42) from ThermoFisher. Mature macrophages were characterized using CD45-PerCP/Cy5.5 (clone HI30, Cat# 304027) and CD14-APC/Cy7 (clone 63D3, Cat# 367108) from Biolegend, and MerTK-PE (clone 125518, Cat# FAB8912P) from R&D Biosystems. Mouse IgG1-PE isotype control for MerTK staining was Cat# 400111 from Biolegend.

Single Cell RNA Sequencing

All non-adherent cells were harvested on Day 6 or Day 14 of macrophage differentiation and prepared for single cell RNA sequencing using the 3'v2 kit from 10X Genomics, following their published protocol. 10,000 cells per sample were put into the sequencing pipeline. Samples were sequenced on a HiSeq 3000 (Illumina) and read alignment was performed using the 10X Genomics CellRanger pipeline (https://support.10xgenomics.com/single-cell-gene-expression/software/over-view/welcome). Downstream analyses were performed using Seurat R software package version 4.0 (http://satijalab.org/seurat/).

The following pipeline was used for the mature macrophage (Day 14) dataset: The CellRanger counts matrix was filtered using the following QC cutoffs: 1) Genes expressed in fewer than 3 cells; 2) Cells containing fewer than 200 or greater than 5,000 genes were removed as these could be potential doublets; 3) Cells with a mitochondrial content of > 7.5% were removed as these are potentially dying cells. Upon filtering, normalization, variance stabilization, and scaling was performed with mitochondrial percent regression using SCTransform to find 3,000 highly variable genes. Principle component analysis was used to find nearest neighbors and a 2D uniform manifold approximation and projection (UMAP) embedding was computed for all visualization purposes. Differentially expressed genes expression were identified using the FindAllMarkers function between clusters and WNTi and WNTd macrophages. Statistically significant genes (adjusted p-value < 0.05) were used to annotate clusters. Differentially expressed genes between WNTi and WNTd macrophages were used to perform gene set enrichment pathway analyses using WebGestalt with the KEGG functional database (http://www.webgestalt.org/).

The following pipeline was used for the progenitor (Day 6) dataset: The CellRanger counts matrix was filtered using the following QC cutoffs: 1) Genes expressed in fewer than 3 cells; 2) Cells containing fewer than 200 or greater than 7,000 genes were removed as these could be potential doublets; 3) Cells with a mitochondrial content of > 7.5% were removed as these are potentially dying cells. Upon filtering, the following was done for WNTd + WNTi merged, WNTd, and WNTi datasets: normalization, variance stabilization, and scaling was performed with mitochondrial percent/cell

cycle regression using SCTransform to find 3,000 highly variable genes. Principle component analysis was used to find nearest neighbors and a 2D uniform manifold approximation and projection (UMAP) embedding was computed for all visualization purposes. FindAllMarkers function in Seurat was used to perform differential gene expression testing between clusters and canonical genes were used for annotation as highlighted by violin plots, heatmaps, and feature plots. Additionally, GeneSet z-scores were calculated for groups of genes to highlight distinct cell states. All scripts used to analyze the data herein are available on GitHub (https://github.com/jamrute/2021_MacDiff_Bredemeyer_Lavine).

Cell types present in each cluster were determined by comparing gene expression signatures with profiles in BloodSpot (Bagger, Kinalis, and Rapin 2019) and the Human Protein Atlas (https://www.proteinatlas.org/).

Palantir was used to perform all pseudotime trajectory analyses in WNTd and WNTi datasets. SCTransform normalized and scaled counts from the 3,000 most highly variable genes were used as an input into Palantir (https://github.com/dpeerlab/Palantir). For the WNTd dataset, the CD34+ progenitor cluster was used as the starting state and for the WNTi dataset, the progenitor 1 cluster was used as the starting state.

The human fetal liver and yolk sac datasets from (Popescu et al. 2019) were integrated into a single data space using Harmony (Korsunsky et al. 2019). The HSC/MPP clusters from both datasets were then reference mapped onto the WNTd and WNTi progenitor datasets using a Seurat v4 pipeline.

Macrophage Morphological and Functional Analyses

Cells were prepared and imaged by transmission electron microscopy as described in (Dege et al. 2020). Antibodies recognizing CD68 (Cat# 14-0688-82), TREM2 (Cat# PA5-111856) and LYVE1 (Cat# MA5-32512) were all from Thermo Fisher. Protein expression was quantitated on a per cell basis using integrated density of sum projections of 40x confocal z-stacks. Phagocytosis by hPSC-derived macrophages was measured using pHrodo Red *E. Coli* beads (Thermo Fisher). Macrophages were cultured with pHrodo Red beads for one hour, then analyzed for percentage of fluorescent cells by microscopy and intensity of fluorescence by flow cytometry. Assay for phagocytosis of apoptotic thymocytes was performed as described in (Miksa et al. 2009), with co-incubation times of 2h and 5h in 4 well chamber slides (Thermo Fisher). Slides were washed with PBS 3 times to remove non-attached thymocytes, fixed, and stained with anti-CD68 and anti-CD14 (Cat# PA5-13305, Thermo Fisher). Expression of inflammatory genes in hPSC-derived macrophages was measured by qRT-PCR after 4 hours of treatment with either 2.5 or 25 ng/mL lipopolysaccharide (LPS). RNA was isolated using the PureLink RNA Mini Kit (ThermoFisher) and cDNA was generated using the High-Capacity cDNA Reverse Transcription Kit (Thermo Fisher). qRT-PCR was performed using PowerUp Syber Green (Thermo Fisher) and human beta2 microglobulin (B2M) was used as the control gene for dCt comparisons. Primer sequences are as follows: B2M-f (ACTTTGTCACAGCCCAAGATAG); B2M-r(GCAAGCAAGCAGAATTTGGAA); IL-1B-f (ATGGACAAGCTGAGGAAGATG); IL1-B-r (CCCATGTGTCGAAGAAGATAGG); TNFa-f (ACTTTGGAGTGATCGGCC); TNFa-r (GCTTGAGGGTTTGCTACAAC); IL-6-f (AAATTCGGTACATCCTCGACGGCA); IL-6-r (AGTGCCTCTTTGCTGCTTTCACAC). Analysis of reactive oxygen species production was performed on $5x10^4$ cells/well using lucigenin as detailed in (Bagaitkar et al. 2017). Mitochondrial analysis was performed on a Seahorse XF96 (Agilent), using $7.5x10^4$ cells/well, and 1.5 μM oligomycin, 0.5 μM FCCP, 0.5 μM rotenone and 0.5 μM antimycin A, as indicated in the Seahorse XF Mitochondrial Stress Test Kit protocol. LPS treatment was 10ng/mL for 18 hours. Unpaired Student's t-test was used for statistical analyses, and all experiments are n=3.

Acknowledgements

All scRNAseq samples were prepared and sequenced at the McDonnell Genome Institute at the Washington University School of Medicine. Flow cytometry and FACS sorting was carried out at the Flow Cytometry and Fluorescence Activated Cell Sorting Core Facility at the Washington University School of Medicine. Electron microscopy was performed at the Washington University Center for Cellular Imaging. The authors thank the Haniffa lab for sharing their human scRNAseq datasets.

Competing Interests

No competing interests declared.

Funding

This work was supported by the National Institutes of Health (HL138466, HL139714, HL156349, AI148877), the Children's Discovery Institute (PM-LI-2019-829) and the Leducq Foundation (20CVD02).

Data Availability

All scRNAseq data will be uploaded to GEO at time of publication.

References

Ajami, B., J. L. Bennett, C. Krieger, W. Tetzlaff, and F. M. Rossi. 2007. 'Local self-renewal can sustain CNS microglia maintenance and function throughout adult life', *Nat Neurosci*, 10: 1538-43.

Back, M., A. Sultan, O. Ovchinnikova, and G. K. Hansson. 2007. '5-Lipoxygenase-activating protein: a potential link between innate and adaptive immunity in atherosclerosis and adipose tissue inflammation', *Circ Res*, 100: 946-9.

Bagaitkar, J., E. A. Barbu, L. J. Perez-Zapata, A. Austin, G. Huang, S. Pallat, and M. C. Dinauer. 2017. 'PI(3)P-p40phox binding regulates NADPH oxidase activation in mouse macrophages and magnitude of inflammatory responses in vivo', *J Leukoc Biol*, 101: 449-57.

Bagger, F. O., S. Kinalis, and N. Rapin. 2019. 'BloodSpot: a database of healthy and malignant haematopoiesis updated with purified and single cell mRNA sequencing profiles', *Nucleic Acids Res*, 47: D881-D85.

Bajpai, G., and K. J. Lavine. 2019. 'Isolation of Macrophage Subsets and Stromal Cells from Human and Mouse Myocardial Specimens', *J Vis Exp*.

Bajpai, G., C. Schneider, N. Wong, A. Bredemeyer, M. Hulsmans, M. Nahrendorf, S. Epelman, D. Kreisel, Y. Liu, A. Itoh, T. S. Shankar, C. H. Selzman, S. G. Drakos, and K. J. Lavine. 2018. 'The human heart contains distinct macrophage subsets with divergent origins and functions', *Nat Med*, 24: 1234-45.

Bian, Z., Y. Gong, T. Huang, C. Z. W. Lee, L. Bian, Z. Bai, H. Shi, Y. Zeng, C. Liu, J. He, J. Zhou, X. Li, Z. Li, Y. Ni, C. Ma, L. Cui, R. Zhang, J. K. Y. Chan, L. G. Ng, Y. Lan, F. Ginhoux, and B. Liu. 2020. 'Deciphering human macrophage development at single-cell resolution', *Nature*, 582: 571-76.

Boelte, K. C., L. E. Gordy, S. Joyce, M. A. Thompson, L. Yang, and P. C. Lin. 2011. 'Rgs2 mediates pro-angiogenic function of myeloid derived suppressor cells in the tumor microenvironment via upregulation of MCP-1', *PLoS One*, 6: e18534.

Byrum, R. S., J. L. Goulet, R. J. Griffiths, and B. H. Koller. 1997. 'Role of the 5-lipoxygenase-activating protein (FLAP) in murine acute inflammatory responses', *J Exp Med*, 185: 1065-75.
Cochain, C., E. Vafadarnejad, P. Arampatzi, J. Pelisek, H. Winkels, K. Ley, D. Wolf, A. E. Saliba, and A. Zernecke. 2018. 'Single-Cell RNA-Seq Reveals the Transcriptional Landscape and Heterogeneity of Aortic Macrophages in Murine Atherosclerosis', *Circ Res*, 122: 1661-74.
Collison, J. 2018. 'MMP12 makes the cut', *Nat Rev Rheumatol*, 14: 501.
Corjay, M. H., M. A. Kearney, D. A. Munzer, S. M. Diamond, and J. K. Stoltenborg. 1998. 'Antiproliferative gene BTG1 is highly expressed in apoptotic cells in macrophage-rich areas of advanced lesions in Watanabe heritable hyperlipidemic rabbit and human', *Lab Invest*, 78: 847-58.
Daemen, S., A. Gainullina, G. Kalugotla, L. He, M. M. Chan, J. W. Beals, K. H. Liss, S. Klein, A. E. Feldstein, B. N. Finck, M. N. Artyomov, and J. D. Schilling. 2021. 'Dynamic Shifts in the Composition of Resident and Recruited Macrophages Influence Tissue Remodeling in NASH', *Cell Rep*, 34: 108626.
Davies, L. C., S. J. Jenkins, J. E. Allen, and P. R. Taylor. 2013. 'Tissue-resident macrophages', *Nat Immunol*, 14: 986-95.
Davies, L. C., C. M. Rice, E. M. Palmieri, P. R. Taylor, D. B. Kuhns, and D. W. McVicar. 2017. 'Peritoneal tissue-resident macrophages are metabolically poised to engage microbes using tissue-niche fuels', *Nat Commun*, 8: 2074.
Deczkowska, A., A. Weiner, and I. Amit. 2020. 'The Physiology, Pathology, and Potential Therapeutic Applications of the TREM2 Signaling Pathway', *Cell*, 181: 1207-17.
Dege, C., K. H. Fegan, J. P. Creamer, M. M. Berrien-Elliott, S. A. Luff, D. Kim, J. A. Wagner, P. D. Kingsley, K. E. McGrath, T. A. Fehniger, J. Palis, and C. M. Sturgeon. 2020. 'Potently Cytotoxic Natural Killer Cells Initially Emerge from Erythro-Myeloid Progenitors during Mammalian Development', *Dev Cell*, 53: 229-39 e7.
Ditadi, A., C. M. Sturgeon, J. Tober, G. Awong, M. Kennedy, A. D. Yzaguirre, L. Azzola, E. S. Ng, E. G. Stanley, D. L. French, X. Cheng, P. Gadue, N. A. Speck, A. G. Elefanty, and G. Keller. 2015. 'Human definitive haemogenic endothelium and arterial vascular endothelium represent distinct lineages', *Nat Cell Biol*, 17: 580-91.
Drissen, R., N. Buza-Vidas, P. Woll, S. Thongjuea, A. Gambardella, A. Giustacchini, E. Mancini, A. Zriwil, M. Lutteropp, A. Grover, A. Mead, E. Sitnicka, S. E. W. Jacobsen, and C. Nerlov. 2016. 'Distinct myeloid progenitor-differentiation pathways identified through single-cell RNA sequencing', *Nat Immunol*, 17: 666-76.
Drissen, R., S. Thongjuea, K. Theilgaard-Monch, and C. Nerlov. 2019. 'Identification of two distinct pathways of human myelopoiesis', *Sci Immunol*, 4.
Ee, M. T., C. Kantores, J. Ivanovska, M. J. Wong, A. Jain, and R. P. Jankov. 2016. 'Leukotriene B4 mediates macrophage influx and pulmonary hypertension in bleomycin-induced chronic neonatal lung injury', *Am J Physiol Lung Cell Mol Physiol*, 311: L292-302.
Epelman, S., K. J. Lavine, A. E. Beaudin, D. K. Sojka, J. A. Carrero, B. Calderon, T. Brija, E. L. Gautier, S. Ivanov, A. T. Satpathy, J. D. Schilling, R. Schwendener, I. Sergin, B. Razani, E. C. Forsberg, W. M. Yokoyama, E. R. Unanue, M. Colonna, G. J. Randolph, and D. L. Mann. 2014. 'Embryonic and adult-derived resident cardiac macrophages are maintained through distinct mechanisms at steady state and during inflammation', *Immunity*, 40: 91-104.
Epelman, S., K. J. Lavine, and G. J. Randolph. 2014. 'Origin and functions of tissue macrophages', *Immunity*, 41: 21-35.
Frame, J. M., K. E. McGrath, and J. Palis. 2013. 'Erythro-myeloid progenitors: "definitive" hematopoiesis in the conceptus prior to the emergence of hematopoietic stem cells', *Blood Cells Mol Dis*, 51: 220-5.
Frank, B., A. Marcu, A. L. de Oliveira Almeida Petersen, H. Weber, C. Stigloher, J. C. Mottram, C. J. Scholz, and U. Schurigt. 2015. 'Autophagic digestion of Leishmania major by host macrophages is associated with differential expression of BNIP3, CTSE, and the miRNAs miR-101c, miR-129, and miR-210', *Parasit Vectors*, 8: 404.
Ginhoux, F., M. Greter, M. Leboeuf, S. Nandi, P. See, S. Gokhan, M. F. Mehler, S. J. Conway, L. G. Ng, E. R. Stanley, I. M. Samokhvalov, and M. Merad. 2010. 'Fate mapping analysis reveals that adult microglia derive from primitive macrophages', *Science*, 330: 841-5.
Grasso, D., A. Ropolo, A. Lo Re, V. Boggio, M. I. Molejon, J. L. Iovanna, C. D. Gonzalez, R. Urrutia, and M. I. Vaccaro. 2011. 'Zymophagy, a novel selective autophagy pathway mediated by VMP1-USP9x-p62, prevents pancreatic cell death', *J Biol Chem*, 286: 8308-24.

Haenseler, W., S. N. Sansom, J. Buchrieser, S. E. Newey, C. S. Moore, F. J. Nicholls, S. Chintawar, C. Schnell, J. P. Antel, N. D. Allen, M. Z. Cader, R. Wade-Martins, W. S. James, and S. A. Cowley. 2017. 'A Highly Efficient Human Pluripotent Stem Cell Microglia Model Displays a Neuronal-Co-culture-Specific Expression Profile and Inflammatory Response', *Stem Cell Reports*, 8: 1727-42.

Hamidzadeh, K., A. T. Belew, N. M. El-Sayed, and D. M. Mosser. 2020. 'The transition of M-CSF-derived human macrophages to a growth-promoting phenotype', *Blood Adv*, 4: 5460-72.

Haque, M., J. K. Kendal, R. M. MacIsaac, and D. J. Demetrick. 2016. 'WSB1: from homeostasis to hypoxia', *J Biomed Sci*, 23: 61.

Hashimoto, D., A. Chow, C. Noizat, P. Teo, M. B. Beasley, M. Leboeuf, C. D. Becker, P. See, J. Price, D. Lucas, M. Greter, A. Mortha, S. W. Boyer, E. C. Forsberg, M. Tanaka, N. van Rooijen, A. Garcia-Sastre, E. R. Stanley, F. Ginhoux, P. S. Frenette, and M. Merad. 2013. 'Tissue-resident macrophages self-maintain locally throughout adult life with minimal contribution from circulating monocytes', *Immunity*, 38: 792-804.

Hoeffel, G., J. Chen, Y. Lavin, D. Low, F. F. Almeida, P. See, A. E. Beaudin, J. Lum, I. Low, E. C. Forsberg, M. Poidinger, F. Zolezzi, A. Larbi, L. G. Ng, J. K. Chan, M. Greter, B. Becher, I. M. Samokhvalov, M. Merad, and F. Ginhoux. 2015. 'C-Myb(+) erythro-myeloid progenitor-derived fetal monocytes give rise to adult tissue-resident macrophages', *Immunity*, 42: 665-78.

Hoeffel, G., and F. Ginhoux. 2015. 'Ontogeny of Tissue-Resident Macrophages', *Front Immunol*, 6: 486.

Honold, L., and M. Nahrendorf. 2018. 'Resident and Monocyte-Derived Macrophages in Cardiovascular Disease', *Circ Res*, 122: 113-27.

Jin, S., G. Zhao, Z. Li, Y. Nishimoto, Y. Isohama, J. Shen, T. Ito, M. Takeya, K. Araki, P. He, and K. Yamamura. 2009. 'Age-related pulmonary emphysema in mice lacking alpha/beta hydrolase domain containing 2 gene', *Biochem Biophys Res Commun*, 380: 419-24.

Kasaai, B., V. Caolo, H. M. Peacock, S. Lehoux, E. Gomez-Perdiguero, A. Luttun, and E. A. Jones. 2017. 'Erythro-myeloid progenitors can differentiate from endothelial cells and modulate embryonic vascular remodeling', *Sci Rep*, 7: 43817.

Kataoka, K., T. Sato, A. Yoshimi, S. Goyama, T. Tsuruta, H. Kobayashi, M. Shimabe, S. Arai, M. Nakagawa, Y. Imai, K. Kumano, K. Kumagai, N. Kubota, T. Kadowaki, and M. Kurokawa. 2011. 'Evi1 is essential for hematopoietic stem cell self-renewal, and its expression marks hematopoietic cells with long-term multilineage repopulating activity', *J Exp Med*, 208: 2403-16.

Katzenelenbogen, Y., F. Sheban, A. Yalin, I. Yofe, D. Svetlichnyy, D. A. Jaitin, C. Bornstein, A. Moshe, H. Keren-Shaul, M. Cohen, S. Y. Wang, B. Li, E. David, T. M. Salame, A. Weiner, and I. Amit. 2020. 'Coupled scRNA-Seq and Intracellular Protein Activity Reveal an Immunosuppressive Role of TREM2 in Cancer', *Cell*, 182: 872-85 e19.

Korsunsky, I., N. Millard, J. Fan, K. Slowikowski, F. Zhang, K. Wei, Y. Baglaenko, M. Brenner, P. R. Loh, and S. Raychaudhuri. 2019. 'Fast, sensitive and accurate integration of single-cell data with Harmony', *Nat Methods*, 16: 1289-96.

Kyriakides, T. R., and S. Maclauchlan. 2009. 'The role of thrombospondins in wound healing, ischemia, and the foreign body reaction', *J Cell Commun Signal*, 3: 215-25.

Lavin, Y., D. Winter, R. Blecher-Gonen, E. David, H. Keren-Shaul, M. Merad, S. Jung, and I. Amit. 2014. 'Tissue-resident macrophage enhancer landscapes are shaped by the local microenvironment', *Cell*, 159: 1312-26.

Lavine, K. J., S. Epelman, K. Uchida, K. J. Weber, C. G. Nichols, J. D. Schilling, D. M. Ornitz, G. J. Randolph, and D. L. Mann. 2014. 'Distinct macrophage lineages contribute to disparate patterns of cardiac recovery and remodeling in the neonatal and adult heart', *Proc Natl Acad Sci U S A*, 111: 16029-34.

Lux, C. T., M. Yoshimoto, K. McGrath, S. J. Conway, J. Palis, and M. C. Yoder. 2008. 'All primitive and definitive hematopoietic progenitor cells emerging before E10 in the mouse embryo are products of the yolk sac', *Blood*, 111: 3435-8.

Malik, J., A. R. Kim, K. A. Tyre, A. R. Cherukuri, and J. Palis. 2013. 'Erythropoietin critically regulates the terminal maturation of murine and human primitive erythroblasts', *Haematologica*, 98: 1778-87.

Manz, M. G., T. Miyamoto, K. Akashi, and I. L. Weissman. 2002. 'Prospective isolation of human clonogenic common myeloid progenitors', *Proc Natl Acad Sci U S A*, 99: 11872-7.

Mass, E., I. Ballesteros, M. Farlik, F. Halbritter, P. Gunther, L. Crozet, C. E. Jacome-Galarza, K. Handler, J. Klughammer, Y. Kobayashi, E. Gomez-Perdiguero, J. L. Schultze, M. Beyer, C. Bock, and F. Geissmann. 2016. 'Specification of tissue-resident macrophages during organogenesis', *Science*, 353.

McGrath, K. E., J. M. Frame, K. H. Fegan, J. R. Bowen, S. J. Conway, S. C. Catherman, P. D. Kingsley, A. D. Koniski, and J. Palis. 2015. 'Distinct Sources of Hematopoietic Progenitors Emerge before HSCs and Provide Functional Blood Cells in the Mammalian Embryo', *Cell Rep*, 11: 1892-904.

Miksa, M., H. Komura, R. Wu, K. G. Shah, and P. Wang. 2009. 'A novel method to determine the engulfment of apoptotic cells by macrophages using pHrodo succinimidyl ester', *J Immunol Methods*, 342: 71-7.

Minutti, C. M., R. V. Modak, F. Macdonald, F. Li, D. J. Smyth, D. A. Dorward, N. Blair, C. Husovsky, A. Muir, E. Giampazolias, R. Dobie, R. M. Maizels, T. J. Kendall, D. W. Griggs, M. Kopf, N. C. Henderson, and D. M. Zaiss. 2019. 'A Macrophage-Pericyte Axis Directs Tissue Restoration via Amphiregulin-Induced Transforming Growth Factor Beta Activation', *Immunity*, 50: 645-54 e6.

Murray, P. J., and T. A. Wynn. 2011. 'Protective and pathogenic functions of macrophage subsets', *Nat Rev Immunol*, 11: 723-37.

Ng, E. S., L. Azzola, F. F. Bruveris, V. Calvanese, B. Phipson, K. Vlahos, C. Hirst, V. J. Jokubaitis, Q. C. Yu, J. Maksimovic, S. Liebscher, V. Januar, Z. Zhang, B. Williams, A. Conscience, J. Durnall, S. Jackson, M. Costa, D. Elliott, D. N. Haylock, S. K. Nilsson, R. Saffery, K. Schenke-Layland, A. Oshlack, H. K. Mikkola, E. G. Stanley, and A. G. Elefanty. 2016. 'Differentiation of human embryonic stem cells to HOXA(+) hemogenic vasculature that resembles the aorta-gonad-mesonephros', *Nat Biotechnol*, 34: 1168-79.

Palis, J., K. E. McGrath, and P. D. Kingsley. 1995. 'Initiation of hematopoiesis and vasculogenesis in murine yolk sac explants', *Blood*, 86: 156-63.

Palis, J., S. Robertson, M. Kennedy, C. Wall, and G. Keller. 1999. 'Development of erythroid and myeloid progenitors in the yolk sac and embryo proper of the mouse', *Development*, 126: 5073.

Palis, J., and M. C. Yoder. 2001. 'Yolk-sac hematopoiesis: the first blood cells of mouse and man', *Exp Hematol*, 29: 927-36.

Pina, C., G. May, S. Soneji, D. Hong, and T. Enver. 2008. 'MLLT3 regulates early human erythroid and megakaryocytic cell fate', *Cell Stem Cell*, 2: 264-73.

Popescu, D. M., R. A. Botting, E. Stephenson, K. Green, S. Webb, L. Jardine, E. F. Calderbank, K. Polanski, I. Goh, M. Efremova, M. Acres, D. Maunder, P. Vegh, Y. Gitton, J. E. Park, R. Vento-Tormo, Z. Miao, D. Dixon, R. Rowell, D. McDonald, J. Fletcher, E. Poyner, G. Reynolds, M. Mather, C. Moldovan, L. Mamanova, F. Greig, M. D. Young, K. B. Meyer, S. Lisgo, J. Bacardit, A. Fuller, B. Millar, B. Innes, S. Lindsay, M. J. T. Stubbington, M. S. Kowalczyk, B. Li, O. Ashenberg, M. Tabaka, D. Dionne, T. L. Tickle, M. Slyper, O. Rozenblatt-Rosen, A. Filby, P. Carey, A. C. Villani, A. Roy, A. Regev, A. Chedotal, I. Roberts, B. Gottgens, S. Behjati, E. Laurenti, S. A. Teichmann, and M. Haniffa. 2019. 'Decoding human fetal liver haematopoiesis', *Nature*, 574: 365-71.

Puranik, A. S., I. A. Leaf, M. A. Jensen, A. F. Hedayat, A. Saad, K. W. Kim, A. M. Saadalla, J. R. Woollard, S. Kashyap, S. C. Textor, J. P. Grande, A. Lerman, R. D. Simari, G. J. Randolph, J. S. Duffield, and L. O. Lerman. 2018. 'Kidney-resident macrophages promote a proangiogenic environment in the normal and chronically ischemic mouse kidney', *Sci Rep*, 8: 13948.

Setty, M., V. Kiseliovas, J. Levine, A. Gayoso, L. Mazutis, and D. Pe'er. 2019. 'Characterization of cell fate probabilities in single-cell data with Palantir', *Nat Biotechnol*, 37: 451-60.

Sturgeon, C. M., L. Chicha, A. Ditadi, Q. Zhou, K. E. McGrath, J. Palis, S. M. Hammond, S. Wang, E. N. Olson, and G. Keller. 2012. 'Primitive erythropoiesis is regulated by miR-126 via nonhematopoietic Vcam-1+ cells', *Dev Cell*, 23: 45-57.

Sturgeon, C. M., A. Ditadi, G. Awong, M. Kennedy, and G. Keller. 2014. 'Wnt signaling controls the specification of definitive and primitive hematopoiesis from human pluripotent stem cells', *Nat Biotechnol*, 32: 554-61.

Subramanian Vignesh, K., and G. S. Deepe, Jr. 2017. 'Metallothioneins: Emerging Modulators in Immunity and Infection', *Int J Mol Sci*, 18.

Summers, K. M., S. J. Bush, and D. A. Hume. 2020. 'Network analysis of transcriptomic diversity amongst resident tissue macrophages and dendritic cells in the mouse mononuclear phagocyte system', *PLoS Biol*, 18: e3000859.

Takata, K., T. Kozaki, C. Z. W. Lee, M. S. Thion, M. Otsuka, S. Lim, K. H. Utami, K. Fidan, D. S. Park, B. Malleret, S. Chakarov, P. See, D. Low, G. Low, M. Garcia-Miralles, R. Zeng, J. Zhang, C. C. Goh, A. Gul, S. Hubert, B. Lee, J. Chen, I. Low, N. B. Shadan, J. Lum, T. S. Wei, E. Mok, S. Kawanishi, Y. Kitamura, A. Larbi, M. Poidinger, L. Renia, L. G. Ng, Y. Wolf, S. Jung, T. Onder, E. Newell, T. Huber, E. Ashihara, S. Garel, M. A. Pouladi, and F. Ginhoux. 2017. 'Induced-Pluripotent-Stem-Cell-Derived Primitive Macrophages Provide a Platform for Modeling Tissue-Resident Macrophage Differentiation and Function', *Immunity*, 47: 183-98 e6.

Watanabe, S., M. Alexander, A. V. Misharin, and G. R. S. Budinger. 2019. 'The role of macrophages in the resolution of inflammation', *J Clin Invest*, 129: 2619-28.

Wynn, T. A., A. Chawla, and J. W. Pollard. 2013. 'Macrophage biology in development, homeostasis and disease', *Nature*, 496: 445-55.

Yanez, A., S. G. Coetzee, A. Olsson, D. E. Muench, B. P. Berman, D. J. Hazelett, N. Salomonis, H. L. Grimes, and H. S. Goodridge. 2017. 'Granulocyte-Monocyte Progenitors and Monocyte-Dendritic Cell Progenitors Independently Produce Functionally Distinct Monocytes', *Immunity*, 47: 890-902 e4.

Yang, W., Y. Tao, Y. Wu, X. Zhao, W. Ye, D. Zhao, L. Fu, C. Tian, J. Yang, F. He, and L. Tang. 2019. 'Neutrophils promote the development of reparative macrophages mediated by ROS to orchestrate liver repair', *Nat Commun*, 10: 1076.

Yokomizo, T., N. Watanabe, T. Umemoto, J. Matsuo, R. Harai, Y. Kihara, E. Nakamura, N. Tada, T. Sato, T. Takaku, A. Shimono, H. Takizawa, N. Nakagata, S. Mori, M. Kurokawa, D. G. Tenen, M. Osato, T. Suda, and N. Komatsu. 2019. 'Hlf marks the developmental pathway for hematopoietic stem cells but not for erythro-myeloid progenitors', *J Exp Med*, 216: 1599-614.

Yona, S., K. W. Kim, Y. Wolf, A. Mildner, D. Varol, M. Breker, D. Strauss-Ayali, S. Viukov, M. Guilliams, A. Misharin, D. A. Hume, H. Perlman, B. Malissen, E. Zelzer, and S. Jung. 2013. 'Fate mapping reveals origins and dynamics of monocytes and tissue macrophages under homeostasis', *Immunity*, 38: 79-91.

Zaiss, D. M. W., W. C. Gause, L. C. Osborne, and D. Artis. 2015. 'Emerging functions of amphiregulin in orchestrating immunity, inflammation, and tissue repair', *Immunity*, 42: 216-26.

Zeng, Y., J. He, Z. Bai, Z. Li, Y. Gong, C. Liu, Y. Ni, J. Du, C. Ma, L. Bian, Y. Lan, and B. Liu. 2019. 'Tracing the first hematopoietic stem cell generation in human embryo by single-cell RNA sequencing', *Cell Res*, 29: 881-94.

Zhang, J., and P. A. Ney. 2009. 'Role of BNIP3 and NIX in cell death, autophagy, and mitophagy', *Cell Death Differ*, 16: 939-46.

Zhong, S., L. Li, Y. L. Zhang, L. Zhang, J. Lu, S. Guo, N. Liang, J. Ge, M. Zhu, Y. Tao, Y. C. Wu, and H. Yin. 2019. 'Acetaldehyde dehydrogenase 2 interactions with LDLR and AMPK regulate foam cell formation', *J Clin Invest*, 129: 252-67.

Zhou, F., X. Li, W. Wang, P. Zhu, J. Zhou, W. He, M. Ding, F. Xiong, X. Zheng, Z. Li, Y. Ni, X. Mu, L. Wen, T. Cheng, Y. Lan, W. Yuan, F. Tang, and B. Liu. 2016. 'Tracing haematopoietic stem cell formation at single-cell resolution', *Nature*, 533: 487-92.

Figures

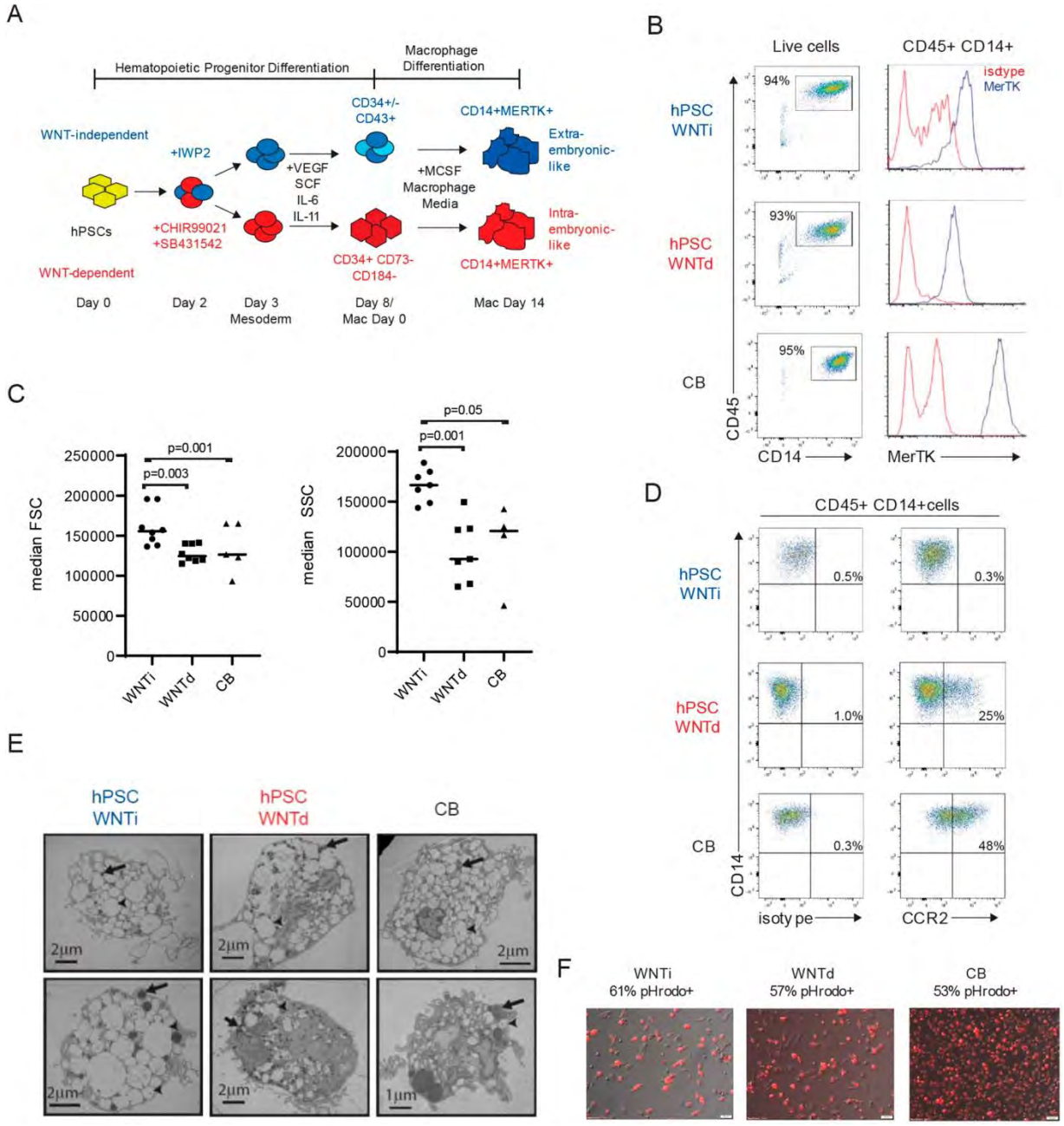

Figure 1. Generation and characterization of WNTi and WNTd hPSC-derived macrophages. A. Schematic of the macrophage differentiation protocol. B. Representative flow cytometric analysis of leukocyte marker CD45 and macrophage markers CD14 and MerTK on WNTi, WNTd and CB cells after 14 days in macrophage media. C. Quantification of median forward scatter (FSC) and side scatter (SSC) of CD14+ cells from 4-7 independent differentiations. Two-tailed Student's t-test. D. Flow cytometric analysis of CCR2 expression on WNTi, WNTd and cord

blood macrophages. Plots are representative of 3 independent experiments. E. Electron microscopy of WNTi, WNTd and CB macrophages. Arrowheads indicate examples of endosomes, arrows indicate examples of lysosomes. F. Phagocytosis of pHrodo Red *E. coli* particles by WNTi, WNTd and CB macrophages after one hour of co-culture, as indicated by red fluorescence. Images shown are merged bright field and fluorescence. At least 100 cells were analyzed per experiment. Pictures shown are representative of 3 independent experiments.

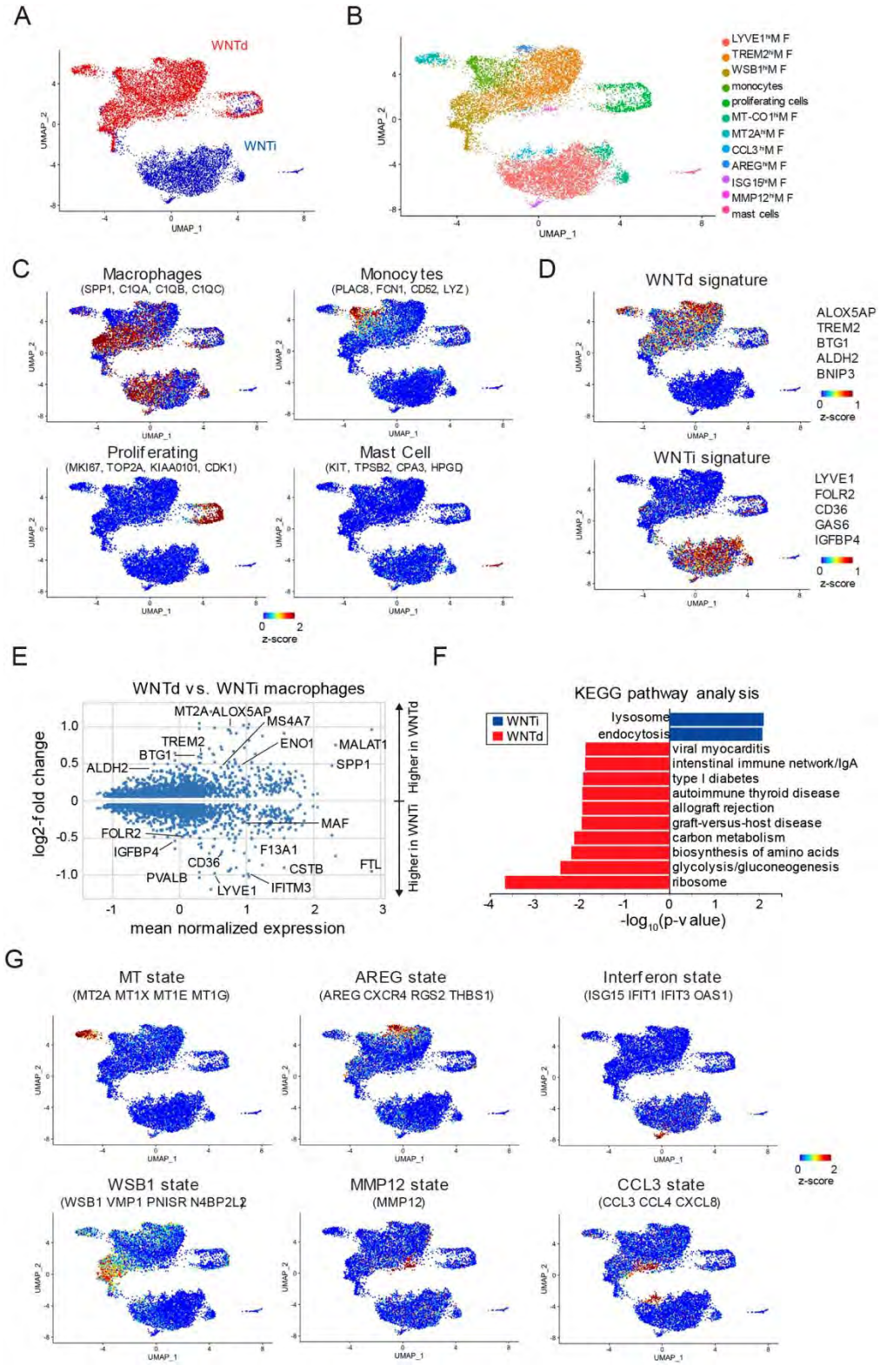

Figure 2. Single cell RNA sequencing of WNTi and WNTd macrophages. A. and B. UMAP plots of WNTd and WNTi macrophage scRNAseq. In (A), WNTi cells are blue and WNTd cells are red. (B) shows the identity of the clusters. Each macrophage (Mϕ) cluster is labeled with the top differentially expressed gene unique to that cluster. C. Z-score feature plots for each distinct cell type (and proliferating cells). Genes used to calculate the z-score are indicated above each plot. D. Z-score feature plots of the WNTd and WNTi macrophage gene signatures. Genes used to calculate the z-score are indicated to the right of the plots. Violin plots of the individual genes are in Fig. S3. E. MA plot of log2 fold-change versus mean normalized gene expression between WNTd and WNTi macrophages. F. Gene set enrichment analysis for KEGG pathway database showing pathways overrepresented in WNTd and WNTi macrophages. G. Z-score feature plots for each macrophage state. The top differentially expressed genes, which are used to generate the z-scores, are indicated above the plots.

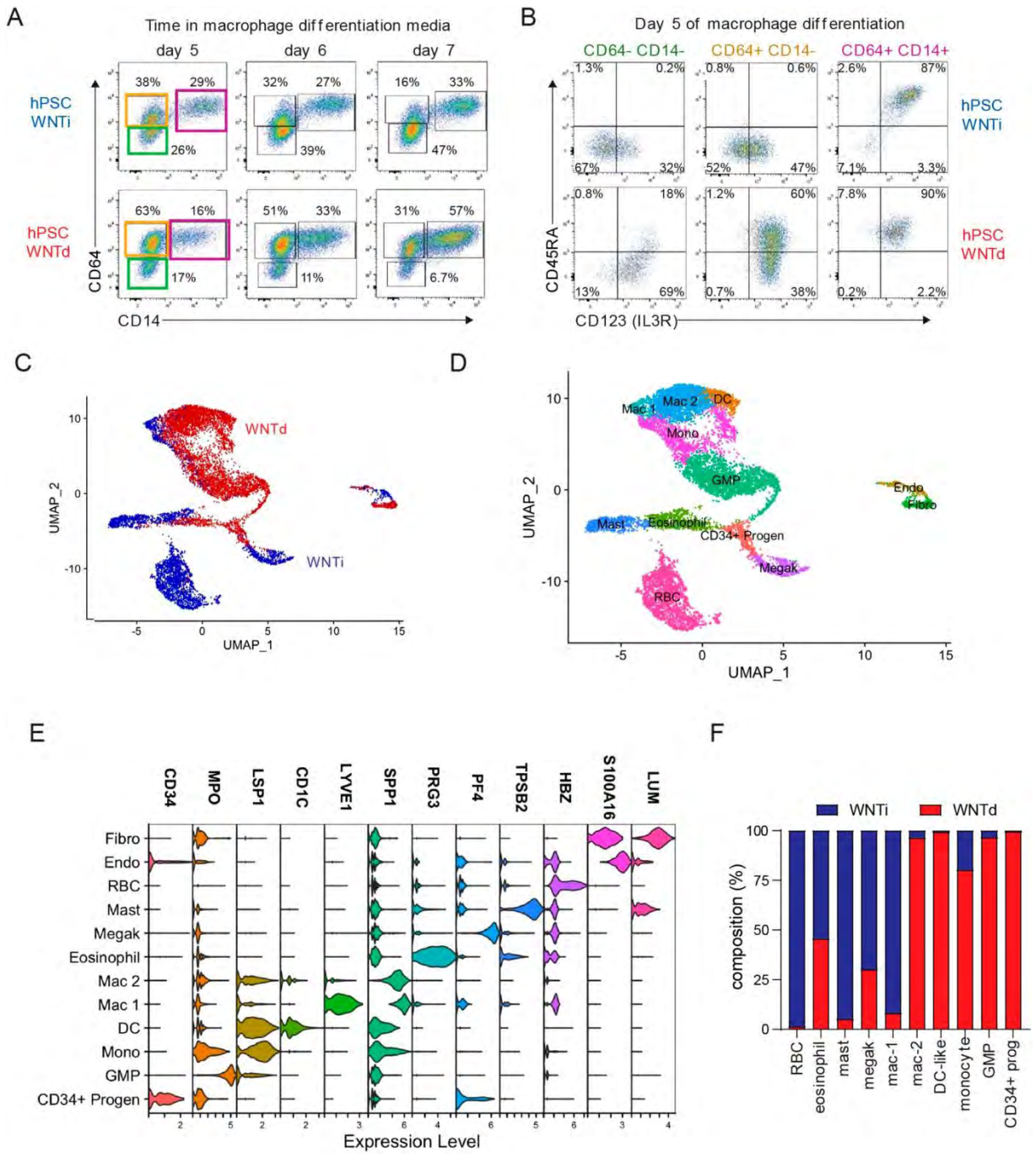

Figure 3. WNTi and WNTd progenitors differ in cell surface markers and downstream cell type potential. A. Representative flow cytometric time course of CD14 and CD64 on WNTi and WNTd progenitors. B. IL-3Rα and CD45RA expression on the indicated populations from the Day 5 plots in (A). C. and D. UMAP plots of WNTi and WNTd progenitor scRNAseq. In (C), WNTi cells and WNTd cells are blue and red, respectively. In (D), clusters are labeled based on expression of cell-type characteristic genes. E. Violin plots of a characteristic gene for each indicated cell type. Additional expression data are shown in Fig. S6 and Table S2. F. The percentage of WNTi and WNTd cells making up each cluster in (D).

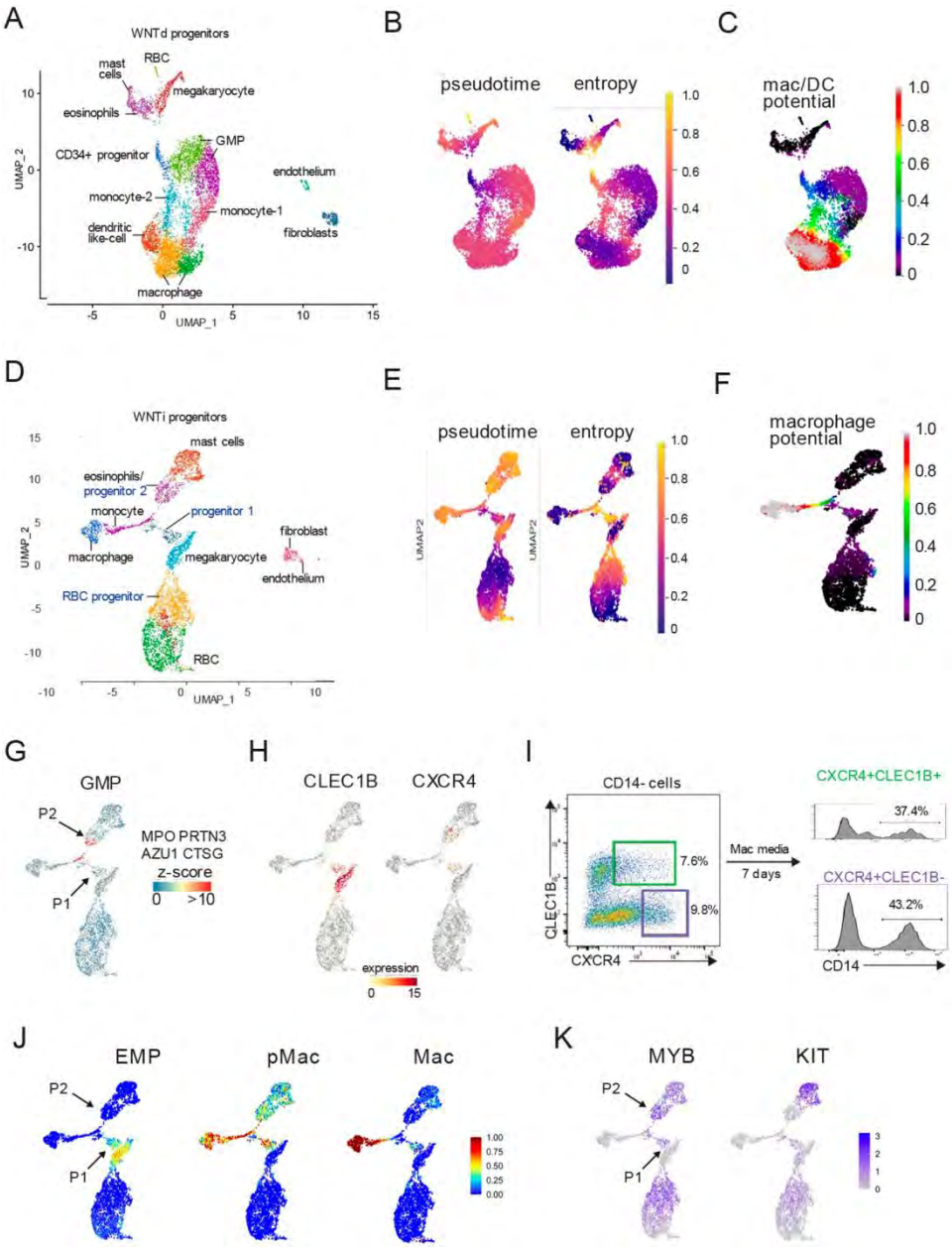

Figure 4. Developmental paths of WNTi and WNTd macrophages. A. scRNAseq UMAP plot of WNTd progenitor culture alone. B. Palantir trajectory analysis of the WNTd progenitors showing pseudotime and entropy (differentiation potential). C. Palantir imputed macrophage potential for all cells in the WNTd progenitor culture. D. scRNAseq UMAP of WNTi progenitor culture alone. E. Palantir trajectory analysis of the WNTi progenitors showing pseudotime and entropy. F. Palantir imputed macrophage potential for all cells in the WNTi progenitor culture. G. Z-score feature plot showing expression of GMP genes in the WNTi cells. Arrows indicate progenitors 1 and 2 (P1 and P2). H. Feature plots of *CLEC1B* and *CXCR4* expression in WNTi cells. I. Flow cytometry plots showing CD14-CXCR4+CLEC1B- and CD14-CXCR4+CLEC1B+ cells in WNTi culture after 4 days in macrophage media. Panels on the right show CD14 expression in these cultures following 7 additional days in macrophage media. Results are representative of 3 independent experiments. J. Z-score plots of EMP, pMac, and macrophage gene signatures from (Mass et al. 2016) in the WNTi cells. Gene lists are in Table S3. K. Feature plots of EMP genes *MYB* and *KIT* in the WNTi progenitors.

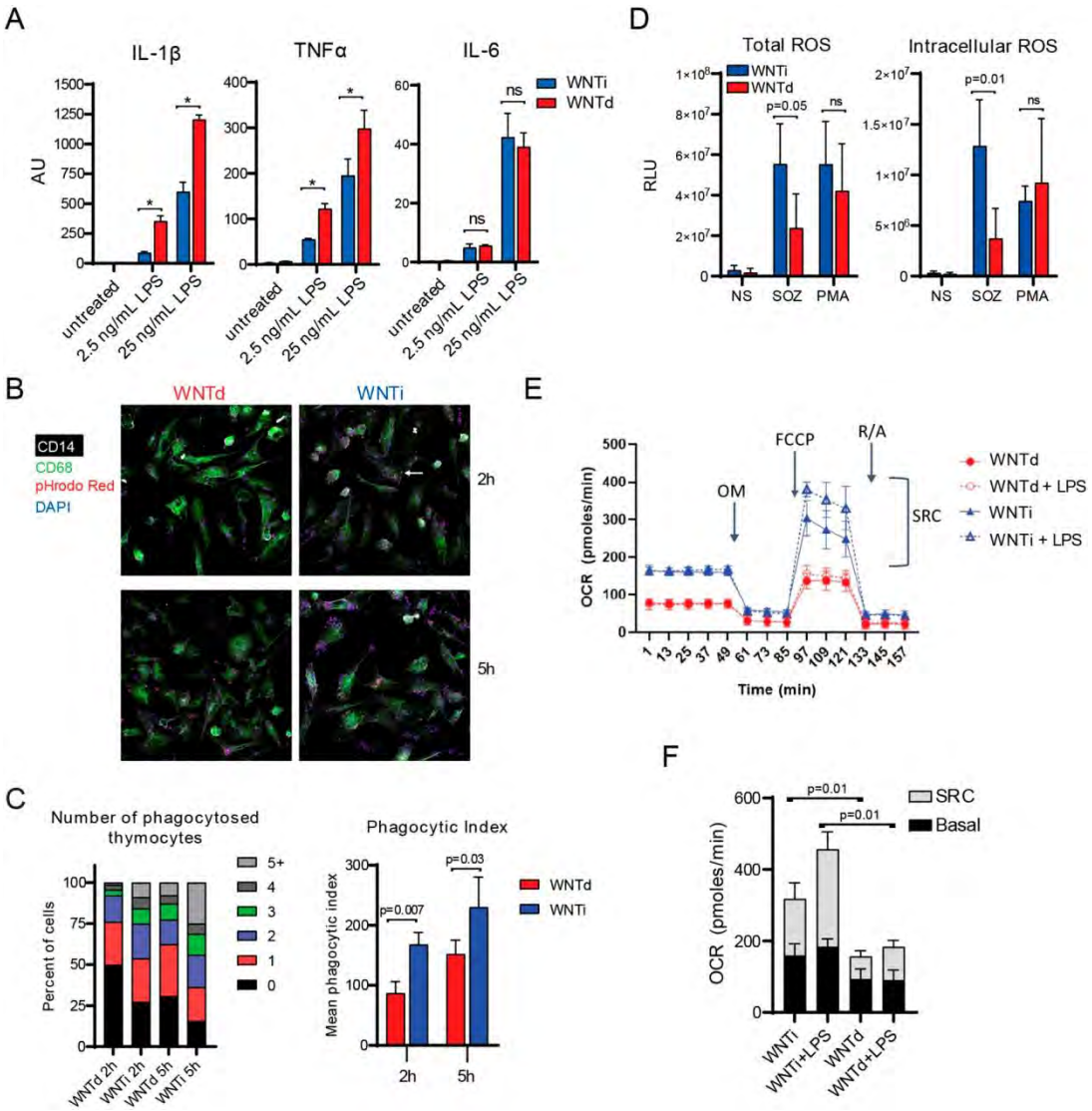

Figure 5. Functional analysis of WNTi and WNTd macrophages. A. Quantitative RT-PCR of *IL-1β, TNFα,* and *IL-6* gene expression of in WNTi and WNTd macrophages after 4 hour treatment with LPS. Asterisk indicates p<0.05, two-tailed Student's t-test; n=3. B. Representative immunofluorescence of phagocytosis of pHrodo Red-labeled apoptotic thymocytes by WNTd and WNTi macrophages. Cells are shown after co-incubation for 2h and 5h. Arrow indicates example of phagocytosed thymocyte. C. Quantification of apoptotic thymocyte phagocytosis by WNTd and WNTi macrophages from three independent differentiations. Left graph shows percentage of macrophages that have phagocytosed thymocytes. Right graph shows mean phagocytic index (% cells with thymocytes x mean thymocytes/cell). Two-tailed Student's t test. D. Production of ROS by WNTi and WNTd macrophages during one hour treatment with SOZ or PMA. Left panel shows total ROS, right panel shows intracellular ROS (superoxide dismutase treated). NS, not stimulated. Two-tailed Student's t-test, n=3. E. OCR in untreated and LPS-treated (10ng/mL) WNTi and WNTd macrophages during Seahorse mitochondrial stress test. Representative of 3 experiments. OM, oligomycin; FCCP, Carbonyl cyanide 4-(trifluoromethoxy)phenylhydrazone; R/A, rotenone/antimycin. F. Quantification of mitochondrial stress tests, using first basal OCR measurement and first measurement following addition of FCCP for calculating SRC. Values are averages from three experiments, +/-SD. Two-tailed Student's t-test.

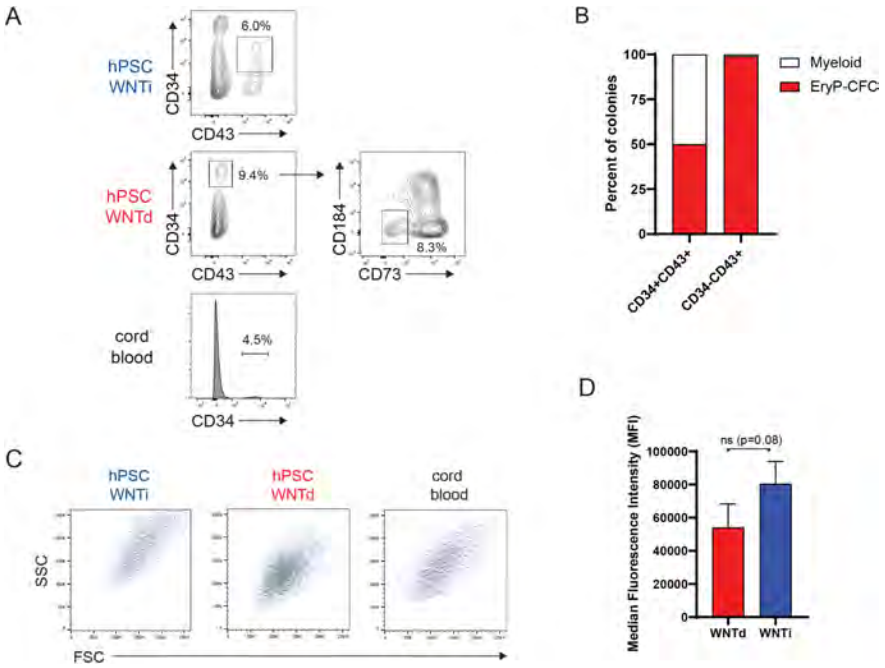

Fig. S1. A. Representative flow cytometric analyses of CD34 and CD43 expression in WNTi and WNTd hematopoietic progenitor cultures on day 8 of differentiation, as well as CD34 expression in human cord blood. B. Erythroid and myeloid potential of CD34+CD43+ and CD34-CD43+ WNTi cell fractions, as determined from numbers of EryP-CFC and CFU-GM colonies, respectively, forming in MethoCult H4034. Percentages are averaged from 3 experiments. C. Representative forward scatter (FSC) and side
scatter (SSC) flow cytometry plots for quantification shown in Fig. 1C. D. Median fluorescence intensity of pHrodoRed in WNTd and WNTi macrophages following 1 hour of incubation with pHrodoRed *E. coli* particles. Results are from three independent macrophage differentiations. Two-tailed Student's t-test.

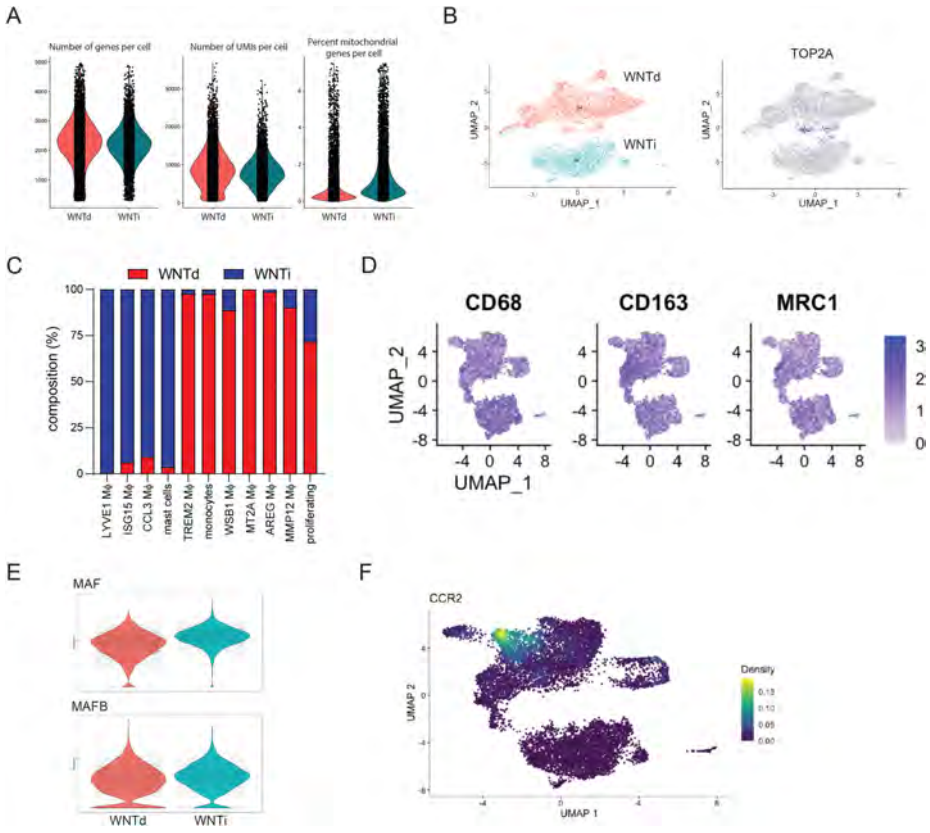

Fig. S2. A. scRNAseq parameters for WNTd and WNTi Day 14 macrophage cultures in Fig. 2. B. UMAP plots of WNTi and WNTd Day 14 macrophage cultures with cell cycle regression, showing that many TOP2A positive cells are still forming a separate cluster after regression. For this reason, this dataset was analyzed without cell cycle regression. C. The percentage of WNTi and WNTd cells making up each cluster in Fig. 2B. D. Feature plots of expression of common macrophage genes in the WNTi and WNTd macrophages. E. Violin plots of expression of macrophage transciption factors *MAF* and *MAFB* in WNTd and WNTi macrophages. F. Density plot of *CCR2* gene expression in the Day 14 macrophage cultures in Fig. 2.

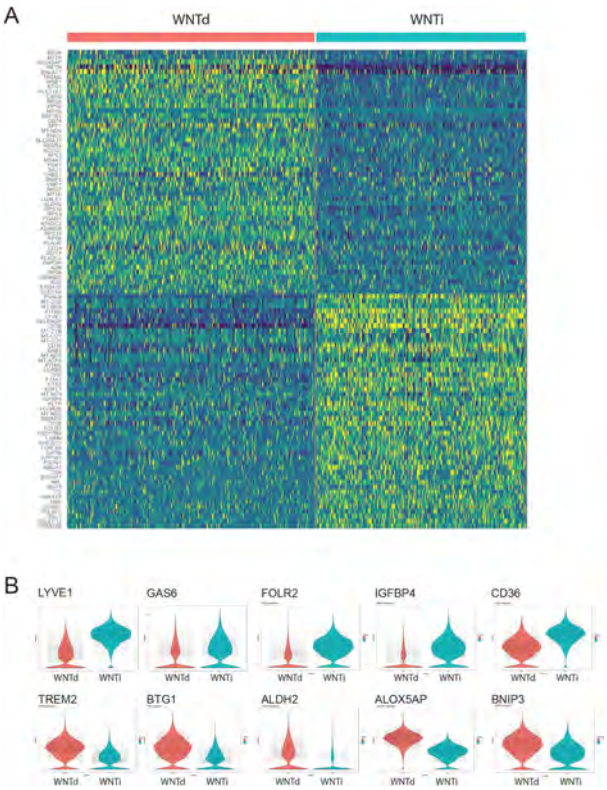

Fig. S3. A. Heat map of the genes with log2 expression difference greater than 0.5 in the WNTd and WNTi macrophage clusters in Fig. 2E. B. Violin plots of the individual genes that make up the WNTi and WNTd macrophage signatures in Fig. 2E.

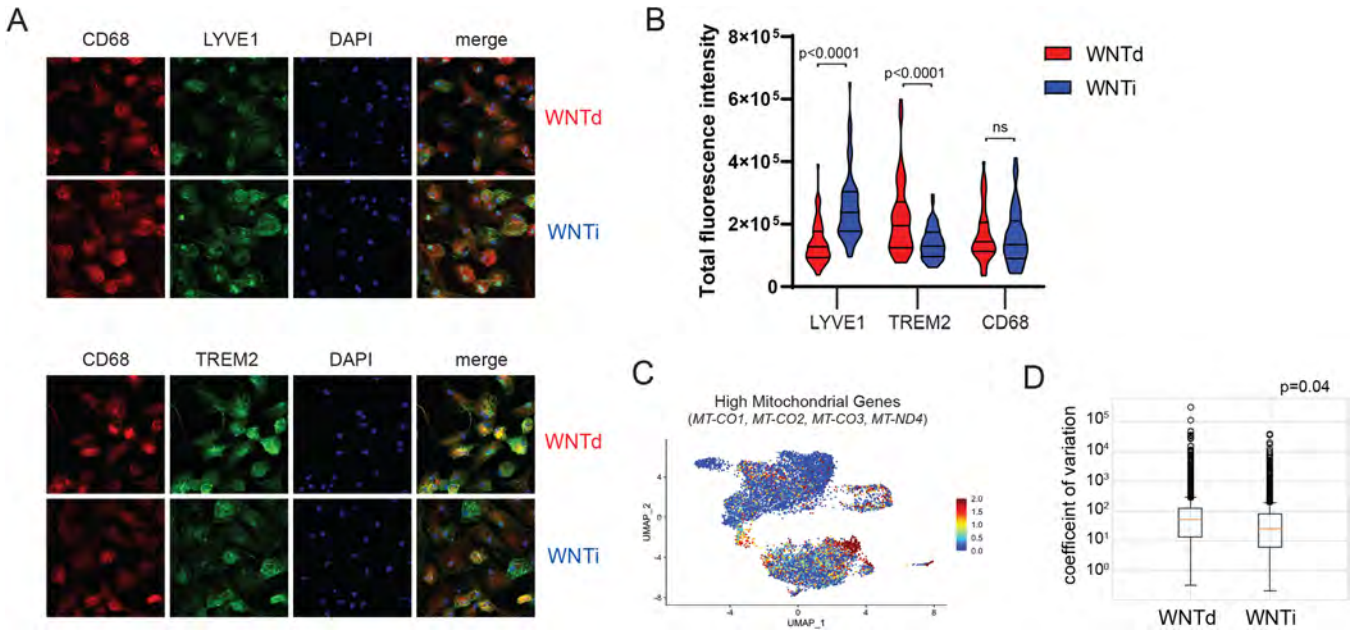

Fig. S4. A. Immunofluorescence images (maximum intensity z-stack projections) of LYVE1 and TREM2 protein expression in WNTi and WNTd macrophages. B. Quantitation of total fluorescense intensity per cell (using sum z-stack projection) for LYVE1, TREM2 and CD68 immunofluorescence. Results are from three independent differentiations, with at least 15 cells per differentiation. Significance calculated using two-tailed student's t test. C. Z-score feature plot of mitochondrial genes overexpressed in the MT-CO2 Mϕ cluster shown in Fig. 2. D. Coefficient of variation (CV) of gene expression for all genes in the WNTd and WNTi macrophages, calculated as CV=StDev expression/mean expression for each gene. The lower CV in the WNTi macrophages indicates that expression of individual genes has a lower dispersion in these cells than in the WNTd macrophages.

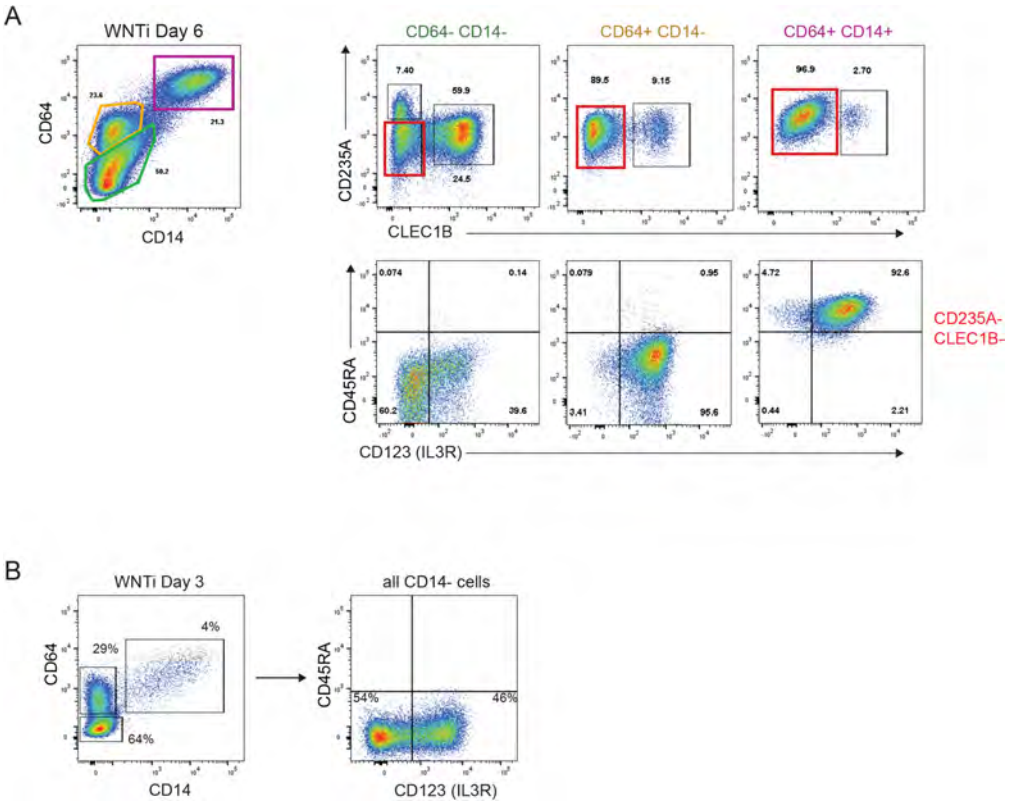

Fig. S5. A. Flow cytometric analysis of IL3R and CD45RA expression on CD235A-CLEC1B- cells in macrophage Day 6 WNTi culture. B. Flow cytometric analysis of IL3R and CD45RA expression in macrophage Day 3 WNTi culure. All plots are representative of 3 independent experiments.

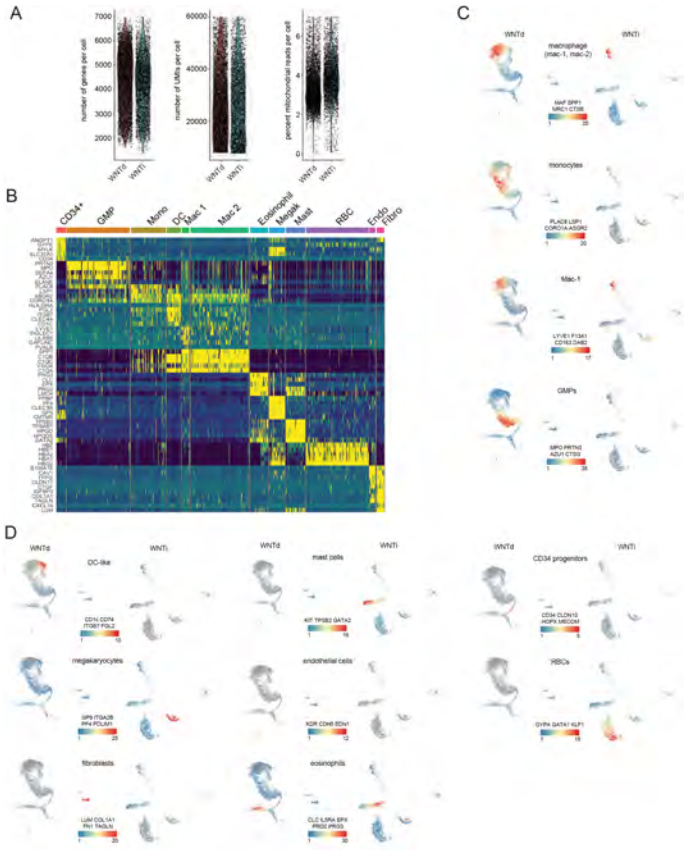

Fig. S6. A. Comparison of scRNAseq parameters for WNTd and WNTi macrophage progenitor samples. B. Heat map of top 5 differentially expressed genes for each scRNAseq cluster in Fig. 3D. C. Z-score feature plots of cell type characteristic genes for macrophage, monocyte and GMP cell clusters in WNTd and WNTi macrophage progenitor scRNAseq analysis shown in Fig. 3. Genes used to calclulate the z-score are indicated below each plot. D. Z-score feature plots for additional cell type clusters shown in Fig. 3. Genes used to calculate the z-score are indicated below each plot.

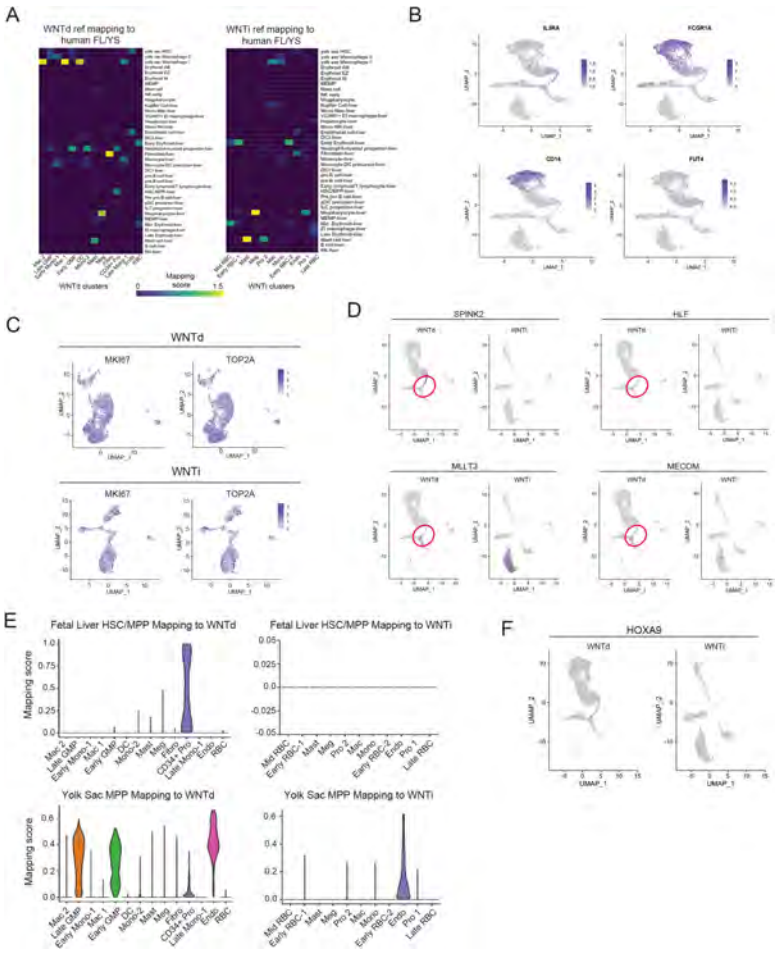

Fig. S7. A. Reference mapping of WNTd and WNTi progenitors to integrated human fetal liver and yolk sac dataset from Popescu, et. al. B. scRNAseq feature plots of cell surface markers used in Fig. 3A and B (*IL3RA, FCGR1A, CD14*), and for neutrophil marker CD15 (*FUT4)*. C. Feature plots of expression of S/G2 markers *MKI67* and *TOP2A* in WNTi and WNTd progenitor cultures. D. Feature plots of expression of *SPINK2, HLF, MLLT3* and *MECOM*. Red circles indicate location of CD34+ WNTd progenitors. E. Reference mapping of human fetal liver HSC/MPPs and yolk sac MPPs onto WNTd and WNTi progenitor populations. F. Feature plots of *HOXA9* expression in WNTd and WNTi progenitor cultures.

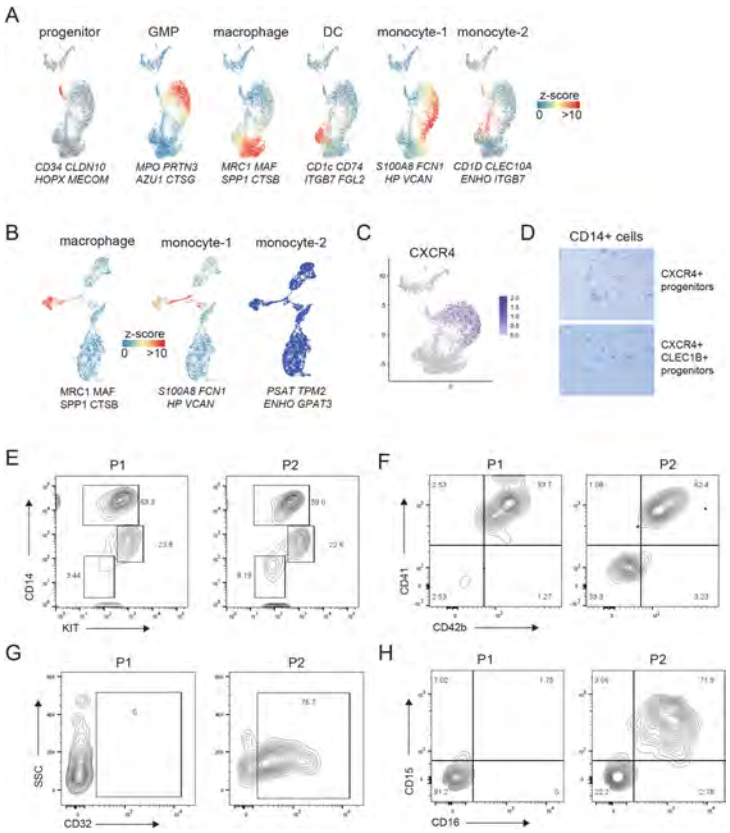

Fig. S8. A. Z-score feature plots of monocyte/macrophage lineage clusters in the WNTd macrophage progenitor scRNAseq analysis shown in Fig. 4. Genes used to calculate the z-scores are indicated below each plot. Genes are the same cell-type characteristic genes shown in Fig. S4, except for the genes used to differentiate monocyte-1 and monocyte-2, which are the top differentially expressed genes in each cluster that are not shared between the two clusters. B. Z-score feature plots of monocyte and macrophage clusters in the WNTi macrophage progenitor scRNAseq analysis shown in Fig. 4. Genes used to calculate the z-scores are indicated below each plot. The monocyte-1 and monocyte-2 genes are the same as in (A), showing that the monocytes in the WNTi culture share a gene expression pattern with the monocyte-1 cluster in the WNTd culture, and do not express the genes characteristic of monocyte-2. C. Feature plot o *CXCR4* gene expression in the WNTd macrophage progenitor culture. D. Brightfield images (representative of two experiments) of CD14+ cells differentiated from CXCR4+ and CXCR4+CLEC1B+ progenitors. E-F. Flow cytometric analysis of progenitor 1 (P1) and progenitor 2 (P2) cultures after 7 days in (E) mast cell and (F) megakaryocyte promoting conditions. Plots in F show only CD14- cells. G-H. Flow cytometric analysis of granulocyte markers CD32 (F) and CD15 and CD16 (G) on CD14- cells isolated from MethoCult H4034. All flow cytometric analyses are representative of two independent experiments.

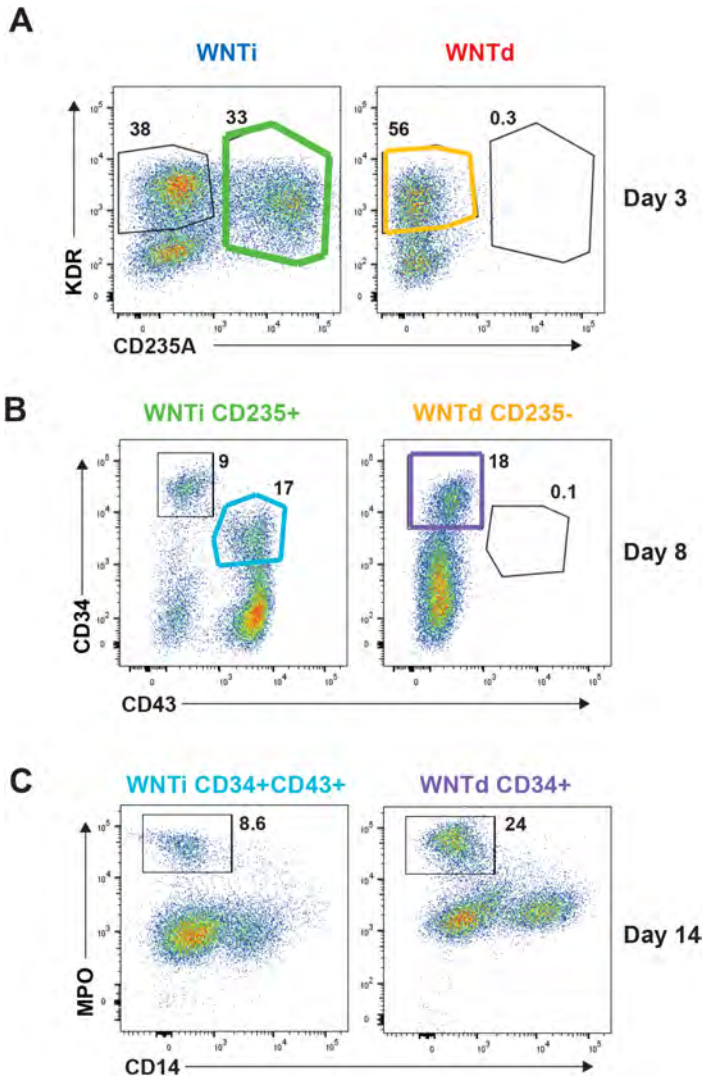

Fig. S9. A. Mesoderm progenitor analysis on Day 3 of hematopoietic progenitor differentiation. WNTd KDR+CD235A-and WNTi KDR+CD235A+ cells were isolated by FACS sorting, reaggregated into embryoid body clusters, then cultured as usual until Day 8. B. Analysis of hematopoietic progenitors derived from populations sorted in (A) on Day 8 of hematopoietic progenitor differentiation. WNTd CD34+CD43- and WNTi CD34+CD43+ cells were FACS sorted and then cultured in macrophage media. C. Analysis of MPO expression in WNTd and WNTi cultures 6 days after populations in (B) were placed into macrophage media.

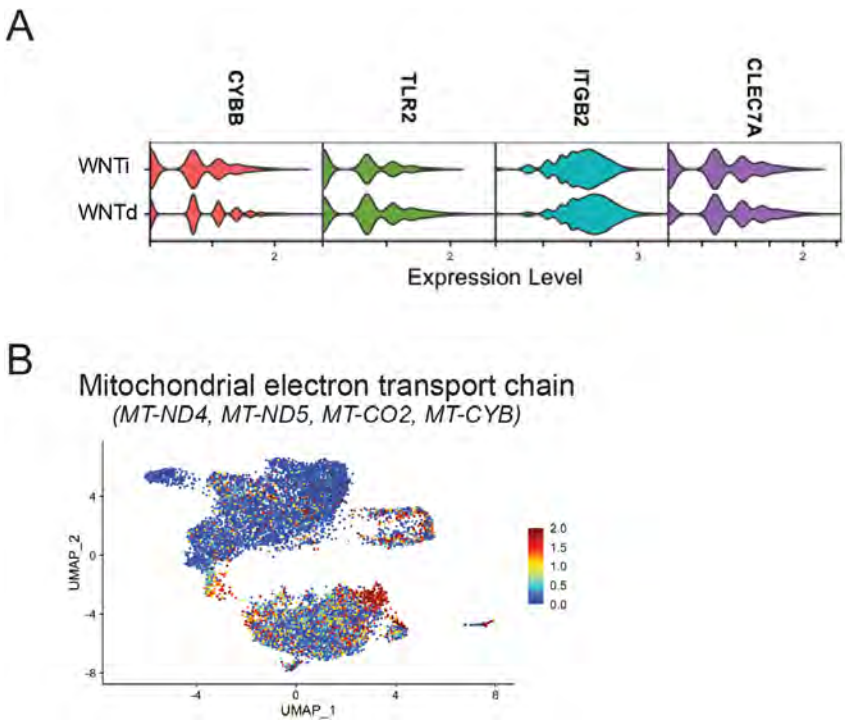

Fig. S10. A. Violin plots of *CYBB, TLR2, ITGB2* and *CLEC7A* expression in WNTd and WNTi macrophages in the macrophage day 14 scRNAseq dataset. B. Z-score feature plot showing mitochondrially encoded genes that have higher expression in WNTi macrophages than WNTd macrophages.

Table S1. scRNAseq data for combined Day 14 WNTd and WNTi mature macrophages

(shown in Figure 2)

Click here to download Table S1

Table S2. scRNAseq data for combined WNTd and WNTi macrophage progenitors

(shown in Figure 3)

Click here to download Table S2

Table S3. Gene signatures for EMP, pre-macrophage (pMac), and macrophage adapted from Mass, et al, Science, 2016.

Click here to download Table S3